Endocrinology, 2021, Vol. 162, No. 8, 1–22
doi:10.1210/endocr/bqab090
Research Article

Research Article

Adrenomedullin Ameliorates Pulmonary Fibrosis by Regulating TGF-ß-Smads Signaling and Myofibroblast Differentiation

Yangxuan Wei,[1] Megumu Tanaka,[1] Takayuki Sakurai,[1,2] Akiko Kamiyoshi,[1,2] Yuka Ichikawa-Shindo,[1] Hisaka Kawate,[1] Nanqi Cui,[1] Shinji Kakihara,[1] Yunlu Zhao,[1] Kohsuke Aruga,[1] Hideki Sanjo,[3] and Takayuki Shindo[1,2]

[1]Department of Cardiovascular Research, Shinshu University School of Medicine, Matsumoto 390-8621, Japan; [2]Department of Life Innovation, Institute for Biomedical Sciences, Interdisciplinary Cluster for Cutting Edge Research, Shinshu University, Matsumoto 390-8621, Japan; and [3]Department of Molecular and Cellular Immunology, Shinshu University School of Medicine, Matsumoto 390-8621, Japan

ORCiD number: 0000-0002-1262-0819 (T. Shindo).

Abbreviations: AM, adrenomedullin; BLM, bleomycin; CLR, calcitonin receptor-like receptor; DMEM, Dulbecco's modified Eagle medium; FACS, fluorescence-activated cell sorting; Fbs, fibroblasts; IL, interleukin; MCP-1, monocyte chemoattractant protein 1; MyoFbs, myofibroblasts; non-p-MyoFbs, nonproliferating myofibroblasts; p-MyoFbs, proliferating myofibroblasts; proto-MyoFbs, proto-myofibroblasts; qPCR, quantitative polymerase chain reaction; RAMP2, receptor activity-modifying protein 2; α-SMA, α-smooth muscle actin; TGF-β, transforming growth factor β; TGFβR1, TGF-β receptor 1; WT, wild-type

Received: 30 March 2021; Editorial Decision: 22 April 2021; First Published Online: 5 May 2021; Corrected and Typeset: 28 June 2021.

Abstract

Pulmonary fibrosis is an irreversible, potentially fatal disease. Adrenomedullin (AM) is a multifunctional peptide whose activity is regulated by receptor activity-modifying protein 2 (RAMP2). In the present study, we used the bleomycin (BLM)-induced mouse pulmonary fibrosis model to investigate the pathophysiological significance of the AM-RAMP2 system in the lung. In heterozygous AM knockout mice (AM+/-), hydroxyproline content and Ashcroft scores reflecting the fibrosis severity were significantly higher than in wild-type mice (WT). During the acute phase after BLM administration, FACS analysis showed significant increases in eosinophil, monocyte, and neutrophil infiltration into the lungs of AM+/-. During the chronic phase, fibrosis-related molecules were upregulated in AM+/-. Notably, nearly identical changes were observed in RAMP2+/-. AM administration reduced fibrosis severity. In the lungs of BLM-administered AM+/-, the activation level of Smad3, a receptor-activated Smad, was higher than in WT. In addition, Smad7, an antagonistic Smad, was downregulated and microRNA-21, which targets Smad7, was upregulated compared to WT. Isolated AM+/- lung fibroblasts showed less proliferation and migration capacity than WT fibroblasts. Stimulation with TGF-β increased the numbers of α-SMA-positive myofibroblasts, which were more prominent among AM+/- cells. TGF-β-stimulated AM+/- myofibroblasts were larger and exhibited greater contractility and extracellular matrix production than WT cells. These cells were α-SMA (+), F-actin (+),

ISSN Online 1945-7170

and Ki-67(-) and appeared to be nonproliferating myofibroblasts (non-p-MyoFbs), which contribute to the severity of fibrosis. Our findings suggest that in addition to suppressing inflammation, the AM-RAMP2 system ameliorates pulmonary fibrosis by suppressing TGF-β-Smad3 signaling, microRNA-21 activity and differentiation into non-p-MyoFbs.

Key Words: adrenomedullin, RAMP2, pulmonary fibrosis, Myofibroblast, TGF-β, Smad, microRNA-21

Idiopathic interstitial pneumonia is an intractable disease in which pulmonary fibrosis gradually progresses over a chronic course in most cases. As respiratory failure worsens, the patient's quality of life is significantly reduced, and the average survival time after diagnosis is reportedly only 3 to 5 years (1, 2). Although several antifibrotic drugs have been launched in recent years, they provide little relief to this group of patients. Consequently, it appears that only by providing patients suffering from idiopathic interstitial pneumonia and pulmonary fibrosis with new therapeutics entailing new mechanisms of action can we improve their prognosis and quality of life.

Adrenomedullin (AM) is a 52-amino acid vasodilating peptide first identified from human pheochromocytoma (3). AM is now known to play important roles in circulatory regulation and the pathogenesis of cardiovascular disease and is a promising therapeutic agent for the treatment of cardiovascular disease. Although AM is mainly secreted in the cardiovascular system, it is widely distributed in numerous tissues and organs (4), where it functions as a local autocrine/paracrine mediator exhibiting anti-inflammatory, anti-oxidative, anti-apoptotic, and antifibrotic effects, among others (5). AM production and secretion are induced by inflammatory cytokines such as tumor necrosis factor-α and interleukin (IL)-1. Conversely, AM induces downregulation of inflammatory cytokines in cultured cells and various animal models (6). In fact, AM is currently undergoing clinical trials in patients with chronic and refractory inflammatory bowel disease (7, 8).

We have generated various mouse knockout models for AM and related molecules. Using those models, we previously observed that homozygous AM knockout (AM-/-) is embryonically lethal midgestation due to systemic edema and bleeding that are mainly caused by abnormal vascular development (9). These observations make it clear that AM is essential for proper development of the vascular system. On the other hand, heterozygous AM knockout (AM+/-) mice survive, although their AM levels are reduced by about half. Interestingly, AM+/- mice are prone to the development of inflammation and fibrosis (10-12). Conversely, transgenic mice overexpressing AM exhibit resistance to various forms of organ damage (9, 13, 14), suggesting AM acts as an anti-inflammatory, anti-fibrotic, and organ-protective factor.

AM is a member of the calcitonin superfamily and acts via a G protein-coupled 7-transmembrane domain receptor, calcitonin receptor-like receptor (CLR) (15). The specificity of CLR for its ligands is regulated by 3 receptor activity-modifying proteins, RAMP1, -2 and -3 (16). Interestingly, among RAMP knockout mice, only homozygous RAMP2 knockout (RAMP2-/-) mice die at midgestation and reproduce the phenotypes observed in AM-/- mice (17). RAMP2 thus appears to be the key determinant of AM's function during vascular development. As conventional RAMP2 knockout is lethal, we generated vascular endothelial cell–specific RAMP2-/- mice. In these mice, we observed marked accumulation of inflammatory cells around blood vessels and, with aging, spontaneous development of organ fibrosis (18). These results suggest that the AM-RAMP2 system is deeply involved in the pathogenesis of inflammation and fibrosis, which in turn raises the possibility of new treatments targeting the activity of the AM-RAMP2 system.

Bleomycin (BLM) is a chemotherapeutic agent used to treat cancer, but one of its side effects is pulmonary toxicity. In the BLM-induced pulmonary fibrosis model, intratracheally administered BLM directly damages alveolar epithelial cells, which leads to infiltration by inflammatory cells and the development of interstitial fibrosis (19). In the present study, we used the BLM-induced pulmonary fibrosis model to evaluate the pathophysiological significance of AM-RAMP2 and to establish a basis for the treatment and prevention of pulmonary fibrosis using AM itself or through regulation of the AM-RAMP2 system.

Methods

Animals

Heterozygous AM (AM+/-) and RAMP (RAMP2+/-) knockout mice were previously generated in our group (9, 17). Wild-type (WT) littermates from each knockout mouse line were used as controls. The background of mice used in this study was C57BL/6J. For time course observation of the BLM-induced pulmonary fibrosis model and experiments entailing exogenous administration of AM, male C57BL/6J mice purchased from Charles River Laboratories Japan (Kanagawa, Japan) were used. All mice were maintained according to a strict procedure under

specific pathogen-free conditions in an environmentally controlled (12-hour light/dark cycle; room temperature, 22 ± 2 °C) breeding room at the Division of Laboratory Animal Research, Department of Life Science, Research Center for Human and Environmental Sciences, Shinshu University. All animal experiments were conducted in accordance with the ethical guidelines of Shinshu University, the Declaration of Helsinki, and the NIH Guide for the Care and Use of Laboratory Animals. All experiments were approved by the Shinshu University Ethics Committee for Animal Experiments. Before all invasive procedures, mice were anesthetized through intraperitoneal injection with a combination of 0.3 mg/kg medetomidine (Nippon Zenyaku Kogyo Co. Ltd., Koriyama Japan), 4.0 mg/kg midazolam (Astellas Pharma Inc. Tokyo Japan), and 5.0 mg/kg butorphanol (Meiji Seika Pharma Co. Ltd., Tokyo Japan).

BLM-Induced Pulmonary Fibrosis Model

Ten- to 12-week-old male AM+/-, RAMP2+/-, and WT mice weighing 25 g were intratracheally instilled with 2 mg/kg BLM (NIPPON KAYAKU, Tokyo, Japan) in 50 µL of sterile saline. The lungs were subsequently removed 3 to 28 days after BLM administration. Left lungs were formalin fixed, paraffin embedded, and used for histological analysis. Right lungs were snap frozen and processed for mRNA. Left lungs were also used for measurement of their hydroxyproline content.

Administration of AM to Mice

Ten- to 12-week-old male C57BL/6J mice weighing 25 g (Charles River Laboratories Japan) were administered recombinant human AM (provided by Dr. Kenji Kangawa) as described previously (20). Using an osmotic pump (Alzet; DURECT Co, Cupertino, CA), mice in the AM-treated group received continuous subcutaneous administration of AM dissolved in sterile saline. The saline-treated group was used as a control. The infusion rate was 0.05 µg/kg/min. Infusion was started 1 day before BLM administration and was continued for an additional 3, 7, or 14 days. The effectiveness of human AM in mice is well established (21, 22), and the dosage used was selected based on earlier studies (23, 24).

Hydroxyproline Assay

Hydroxyproline assays (Quick Zyme Biosciences, Leiden, The Netherlands) were performed as described previously (25). Briefly, left lungs were homogenized in 6 N HCl and hydrolyzed for 20 hours at 95 °C. After hydrolysis, the tubes were cooled to room temperature and then centrifuged for 10 minutes at 13 000 rpm, after which the hydrolyzed samples were diluted with water to 4M HCl, and 35-µl aliquots of standard solution and 4M HCl samples were pipetted into the appropriate wells. Assay buffer was then added and incubated for 20 minutes at room temperature while shaking the plate. A mixture of reagents A and B (2:3) was then added, and the samples were incubated at 60 °C for 60 minutes. After cooling the samples to room temperature, absorbance was measured at 570 nm. The hydroxyproline content was determined against a standard curve generated with pure hydroxyproline.

Fluorescence-Activated Cell Sorting Analysis

Total lungs were minced into 1 mm pieces and digested for 30 minutes at 37 °C with gentle shaking in 20 mL of Hanks' balanced salt solution (HBSS [+]; Wako, Osaka, Japan) supplemented with 0.5 mg/mL collagenase IV (Sigma-Aldrich, St. Louis, MO) and 50 U/ml DNase I (Wako). The resultant single-cell suspensions were then filtered through a cell strainer (mesh 100 µm) (AS ONE, Osaka, Japan), after which they were resuspended in 1 mL of HBSS supplemented with 2% fetal bovine serum and then counted in a microscope counting chamber. After excluding the dead cells using trypan blue, the cell density was adjusted to 1 to 10×10^6 cells/mL. The cells were then centrifuged to remove the supernatant and the Fc Block reaction was run for 10 minutes at 4 °C followed by staining with fluorochrome-conjugated antigen-specific antibodies for 20 minutes at 4 °C in the dark. After resuspending the cells in 700 µL of fluorescence-activated cell sorting (FACS) buffer (1× PBS, 1% BSA, 2nM EDTA, 0.05% NaN3) in a glass tube, 10 µL of 20 µg/mL propidium iodide was added to each the tube.

The regents and fluorochrome-conjugated antibodies used in this research were as follows: TCRβ (H57-597) (RRID: AB_2562562, Cat# 109230) (26), MHC II (M5/114.15.2) (RRID: AB_2290801, Cat# 107629) (27), CD11b (M1/70) (RRID: AB_2629529, Cat# 101263) (28), CD11c (HL3) (RRID: AB_2562414, Cat# 117339) (29), Ly6c (HK1.4) (RRID: AB_2565852, Cat# 128041) (30), Ly6G (1A8) (RRID: AB_1236488, Cat# 127605) (31), and CD4 (RM4-5) (RRID: AB_2563054, Cat# 100548) (32) from BioLegend (San Diego, CA); SiglecF (E50-2440) (RRID: AB_10896143, Cat# 562068) (33) and NK1.1 (PK136) (RRID: AB_10563422, Cat# 561117) (34) from BD Bioscience (San Jose, CA); and CD45 (30-F11) (RRID: AB_1548790, Cat# 47-0451-80) (35) from Thermo Fisher Scientific (Carlsbad, CA). Anti-CD16/CD32 (Mouse Fc Block) (2.4G2) (RRID: AB_394657, Cat# 553142) (36) was from BD Bioscience. Propidium iodide was purchased from Sigma-Aldrich. Stained cells were analyzed using

a FACS Celesta flow cytometer (BD Bioscience). Flow cytometry data were analyzed with Kaluza software (Beckman Coulter, Brea, CA). Gating was performed as shown in Supplementary Figure 1 (37).

Real-Time Quantitative Polymerase Chain Reaction Analysis

Total RNA was prepared using TRI REAGEN (Molecular Research Center, Cincinnati, OH) and a DNA-free DNA Removal kit (Ambion, Naugatuck, CT) according to the manufacturer's instructions. For cDNA synthesis, RNA was reverse transcribed using a High Capacity cDNA Reverse Transcription Kit (Applied Biosystems, Foster City, CA). PCR primers and probes were designed using NCBI Primer-BLAST (https://www.ncbi.nlm.nih.gov/tools/primer-blast/) and were synthesized by Integrated DNA Technologies (Coralville, IA). The primers and probes used are listed in Table 1. Quantitative polymerase chain reaction (qPCR) was performed using SYBR Green (Toyobo, Osaka, Japan) or Realtime PCR Master Mix (Toyobo) and TaqMan probes (MBL, Aichi, Japan) on an ABI Prism 7300 Sequence Detection System (Applied Biosystems). The cycling conditions were 50 °C for 2 minutes and 95 °C for 2 minutes, followed by 40 cycles of 95 °C for 15 seconds and 60 °C for 1 minute. Relative mRNA levels were normalized to mouse glyceraldehyde-3-phosphate dehydrogenase mRNA (Pre-Developed TaqMan assay reagents; Applied Biosystems) and calculated using the comparative cycle threshold method (ΔΔCt).

Real-Time qPCR Analysis of microRNA-21 Expression

A miRNeasy Mini Kit (QIAGEN, Venlo, Nederland) was used to purify the cellular microRNA. The specific primers were as follows: for microRNA-21 (miR-21), 5′-UAGCUUAUCAGACUGAUGUUGA-3′ (mmu-miR-21a-5p, MIMAT0000530, QIAGEN) and for normalization control RNA U6, 5′-GUGCUCGCUUCGGCAGCACAUAUACUAAAAUUGGAACGAUACAGAGAAGAUUAGCAUGGCCCCUGCGCAAGGAUGACACGCAAAUUCGUGAAGCGUUCCAUAUUUUU-3′ (Hs_RNU6-2_11 MS00033740, QIAGEN). For cDNA synthesis, RNA was reverse transcribed using a miScript Reverse Transcription Kit (QIAGEN), and a miScript SYBR Green PCR Kit was used according to the manufacturer's instructions (QIAGEN). Quantitative real-time PCR was performed using a StepOnePlus real-time qPCR system (Thermo Fisher Scientific).

Histological Examination

Lung sections were fixed in 4% formalin neutral buffer, embedded in paraffin, and cut into 4-μm-thick sections. Some sections were used for hematoxylin/eosin (H&E) and Masson trichrome staining. Immunohistochemical staining was performed using anti-CD45 (RRID: AB_357485, Cat# MAB114, Wako, Osaka, Japan) (38), anti-F4/80 (RRID: AB_323806, Cat# MCA497GA, Bio-Rad, Hercules, CA) (39), anti-CD3 (RRID: AB_305055, Cat# ab5690, Abcam, Cambridge, England) (40), and anti-α-SMA (RRID: AB_2223500, Cat# M0851, Dako) (41) antibodies. Biotin-conjugated secondary antibodies and 3,3′-diaminobenzidine (DAB) (Histofine kit, Nichirei, Tokyo, Japan) were used to visualize the labeling of α-SMA, CD3, or F4/80. A VECTASTAIN ABC kit (Vector Laboratories, Burlingame, CA) was used to visualize CD45 labeling, and the nuclei were counterstained with hematoxylin. Inspections were performed using a microscope (BZ-X710; Keyence, Osaka, Japan). Quantification was performed using a BZ analyzer (Keyence).

Modified Ashcroft Score

Pulmonary fibrosis severity was graded using a modified Ashcroft score (42). Based on the histological features of the pulmonary fibrosis, the severity was graded from 0 (Alveolar septa: no fibrotic burden at the most flimsy small fibers in some alveolar walls. Lung structure: Normal lung) to 8 (Alveolar septa: nonexistent. Lung structure: microscope fields show complete obliteration with fibrotic masses).

Western Blot Analysis

Lungs and cells were lysed in an ice-cold RIPA Lysis Buffer System (Santa Cruz Biotechnology, Santa Cruz, CA) supplemented with PosSTOP phosphatase inhibitor (Roche Applied Science, Upper Bavaria, Germany) and then sonicated. Samples of the resultant lysate (1 μg/well for cells, 10 μg/well for lungs) were subjected to electrophoresis in TGX gel (Bio-Rad Laboratories, Hercules, CA), and which the resolved proteins were transferred to PVDF membranes (Bio-Rad Laboratories). After blocking with 5% skim milk, the membranes were probed using primary antibodies against Smad2 (RRID: AB_10626777, Cat# 5339S) (43), Smad3 (RRID: AB_2193182, Cat# 9523S) (44), p-Smad3 (RRID: AB_2193207, Cat# 9520S) (45) (Cell Signaling Technology, Danvers, MA), p-Smad2 (RRID: AB_2889838, Cat# ab184557) (46) and Smad7 (RRID: AB_2889839, Cat# ab216428) (47) (Abcam) all at 1:1000 dilution, followed by appropriate secondary antibodies

Table 1. Primers and probes used for real-time pcr

Adm (adrenomedullin)	Forward	5′-GGACACTGCAGGGCCAGAT-3′
	Reverse	5′-GTAGTTCCCTCTTCCCACGACTTA-3′
Ramp2 (RAMP2)	Probe	5′-CCCAGAGGATGTGCTCCTGGCCAT-3′
	Forward	5′-GCAGCCCACCTTCTCTGATC-3′
	Reverse	5′-AACGGGATGAGGCAGATGG-3′
Ramp3 (RAMP3)	Forward	5′-AAAGCCTTCGCTGACATGATG-3′
	Reverse	5′-ATCTCGGTGCAGTTAGTGAAGCT-3′
Calcrl (CLR)	Probe	5′-ATCGTGGTGGCTGTGTTTGCGGAG-3′
	Forward	5′-AGGCGTTTACCTGCACACACT-3′
	Reverse	5′-CAGGAAGCAGAGGAAACCCC-3′
Il-6 (IL-6)	Forward	5′-CTGCAAGAGACTTCCATCCAGTT-3′
	Reverse	5′-GAAGTAGGGAAGGCCGTGG-3′
Ccl2 (MCP-1)	Forward	5′-GCAGTTAACGCCCCACTCA-3′
	Reverse	5′-CCTACTCATTGGGATCATCTTGCT-3′
Col1a1 (Type I collagen α1)	Forward	5′-ATGGATTCCCGTTCGAGTACG-3′
	Reverse	5′-TCAGCTGGATAGCGACATCG-3′
Spp1 (Osteopontin)	Probe	5′-CCCAGCTTCTGAGCATGCCCTCTG-3′
	Forward	5′-CCCTCGATGTCATCCCTGTT-3′
	Reverse	5′-CCCTTTCCGTTGTTGTCCTG-3′
Fn1 (Fibronectin)	Forward	5′-GGCTACATCATCCGCCATCA-3′
	Reverse	5′-GCCCGGATTAAGGTTGGTGA-3′
Acta2 (α-SMA)	Forward	5′-CCACCGCAAATGCTTCTAAGT-3′
	Reverse	5′-GGCAGGAATGATTTGGAAAGG-3′
Tgfb1 (TGF-β1)	Forward	5′-CCCGAAGCGGACTACTATGC-3′
	Reverse	5′-TAGATGGCGTTGTTGCGGT-3′
Timp1 (TIMP-1)	Forward	5′-CCGCCTAAGGAACGGAAATT-3′
	Reverse	5′-GGGCTCAGAGTACGCCAGG-3′
Islr (Meflin)	Forward	5′-AGATCCGCTCGGTGGCTATT-3′
	Reverse	5′-AGGTCGCTCCAGGCAAACT-3′

(Santa Cruz). Anti-β-actin antibody (RRID: AB_2223172, Cat# 4970S, Cell Signaling Technology) (48) at 1:8000 dilution served as a loading control. The bound antibodies were visualized using chemiluminescent horseradish peroxidase substrate (Merck Millipore, Burlington, MA), and the chemiluminescence was analyzed using an Image Quant LAS 4000 system (GE Healthcare). Levels of Smad2 and Smad3 activation were determined based on the ratio of band intensities after blotting with antibodies specific for the phosphorylated and unphosphorylated proteins. For quantification, images of the blots were captured and analyzed using Image Quant TL software (GE Healthcare).

Isolation of Lung Fibroblasts

Mouse lung fibroblasts were established as described previously (49). Fresh tissue samples collected from lungs were washed with serum-free Dulbecco's modified Eagle medium (DMEM; Wako), finely minced into small pieces of approximately 0.5 to 1.0 mm and digested enzymatically with 2 mg/mL collagenase type I (Wako) in DMEM for 3 hours at 37 °C. After cell dissociation, the samples were filtered through a cell strainer (mesh 40 μm) (AS ONE, Osaka, Japan), centrifuged, washed with PBS and cultured in 3.5 cm dishes in DMEM supplemented with 10% fetal bovine serum and 1% penicillin-streptomycin. Cells were allowed to grow on the plate for 4 days. During that period, the medium was replenished every 2 days. To ensure minimal contamination by epithelial cells prior to their use in experiments, the cells were tested to confirm >95% positive staining for vimentin and negative staining for E-cadherin. Primary cultured pulmonary fibroblasts with 3 to 4 passages were used for experiments.

TGF-β-Stimulation of Primary Cultured Lung Fibroblasts

Cultured lung fibroblasts were pretreated with AM (10^{-7} M) or PBS for 2 hours followed by treatment with transforming growth factor-β1 (TGF-β1) (10 ng/mL) for 24 hours. The dosage and treatment period were chosen based on previous studies (50-52). In some experiments, the cells were also treated for 24 hours with 10 μM SB431542 (Cayman Chemical, Ann Arbor, MI), a selective TGF-β receptor 1 (TGFβR1) inhibitor (53). Alternatively, cells were pretreated with 3μM SIS3 (Merck, Darmstadt, Germany),

a selective Smad3 inhibitor (54), for 1 hour followed by treatment with TGF-β1 (10 ng/mL) for 24 hours (54).

For immunostaining, plates were dipped in 4% paraformaldehyde for 10 minutes, blocked, and immunostained with anti-α-SMA (Code# M0851, Dako) (41), anti-vimentin (RRID: AB_10562134, Cat# ab92547, Abcam) (55), or anti-Ki67 (RRID: AB_443209, Cat# ab15580, Abcam) (56) antibodies. Cells were also stained with phalloidin (Thermo Fisher Scientific) to visualize actin fibers. Nuclei were counterstained using DAPI (Thermo Fisher Scientific). Cells were then examined under a fluorescence microscope (BZ-X710). Positive areas were determined using Hybrid Cell Count (BZ analyzer) under the same conditions.

Gel Contraction Assay

Collagen gel contraction assays were performed according to the manufacturer's instructions (Cell Biolabs; San Diego, CA) (57). Briefly, cells were pretreated for 2 hours with AM (10^{-7} M) or PBS followed by stimulation for 24 hours with TGF-β1 (10 ng/mL). The cells were then collected from plates and suspended at a density of 4.0×10^5 cells per 100 µL of medium to which 400 µL of neutralized collagen solution were added. The resultant mixture was added to one well of a 24-well culture plate and allowed to gel for 2 hours at 37 °C. After polymerization, 1.0 mL of culture medium was added on top of the gel lattice and incubated for 24 hours. The stress was then released by running a sterile pipette tip along the sides of the well. Twelve hours after the stress was released, the culture dish was scanned, and the area of the collagen gel was measured using ImageJ software version 1.53f (NIH, Bethesda, MD; http://imagej.nih.gov/ij).

Cell Proliferation Assay

One hundred-microliter aliquots of fibroblasts suspended at a density of 5×10^4 cells/mL in DMEM containing 10% fetal bovine serum were plated in 96-well plates and incubated for 24 hours. The cells were then treated with 10 ng/mL TGF-β1 for 24 hours, after which the culture medium was changed and 10 µL of Cell Counting Kit-8 (CCK-8) solution (Dojindo, Kumamoto, Japan) were added to each well. The plate was then incubated for 1 hours at 37 °C in an incubator, and the absorbance at 450 nm was measured using a microplate reader. Experiments were performed 4 times independently.

Scratch Assay

For scratch assays, cells were plated in 6-well plates at 2×10^5 cells/well, treated with TGF-β1 (10 ng/mL) and grown into a monolayer. The assays were performed as described previously (58). Briefly, 5 µg/mL mitomycin C (Kyowa Kirin, Tokyo, Japan) was added to the medium for 3 hours to block cell proliferation, and a linear scratch/wound was made on the cell monolayer using a sterile pipette. Photomicrographs were taken of the culture at 40× magnification, and the distance migrated was observed within appropriate times. The distances were measured using CellSens standard software (OLYMPUS, Tokyo, Japan). Experiments were performed 3 times independently.

Downregulation of miR-21

Downregulation of miR-21 was performed as described previously (59). The miR-21 inhibitor LNA-5′-UCAACAUCAGUCUGAUAAGCUA-3′, a chemically modified and optimized oligonucleotide designed to specifically target the microRNA molecule in cells, and its negative control, LNA-5′-CAGUACUUUUGUGUAGUACAA-3′, were purchased from Genepharma (Shanghai, China). Cells were transfected with the oligonucleotides using Lipofectamine 3000 (Thermo Fisher Scientific) at a final concentration of 100nM following the manufacturer's instructions. The efficiency of transfection was assessed with miR-21 qPCR (StepOnePlus real-time PCR system, Thermo Fisher Scientific) and fluorescence microscopy (BZ-X710).

Statistics

Statistical analysis was performed with GraphPad Prism software version 7.03. (GraphPad Software Inc., San Diego, CA). Quantitative values are expressed as the mean ± SEM. The significance of differences was assessed using Student's *t* test, 1-way ANOVA with Tukey's or Dunnett's test, or 2-way ANOVA with Tukey's test. Values of $P < 0.05$ were considered significant. "*" indicates comparison between the groups, "#" indicates comparison with control WT mice, and "†" indicates comparison with control knockout mice. *, #, † indicate $P < 0.05$; **, ##, †† indicate $P < 0.01$; and ***, ###, ††† indicate $P < 0.001$.

Results

Time Course of the Pathogenesis of BLM-Induced Pulmonary Fibrosis

C57BL/6J WT mice were intratracheally administered BLM to induce pulmonary fibrosis. Lung weights and lung weight to body weight ratios were increased from day 3 to day 14 after BLM administration (Supplementary Figure 2A-2C) (37). The expression of genes encoding CLR, AM's receptor, and RAMP2 and

RAMP3 (*Calcrl*, *Ramp2*, and *Ramp3*) gradually declined over the 28-day observation period after BLM administration (Supplementary Figure 2D) (37). Expression of the gene encoding AM (*Adm*) was transiently and significantly elevated on day 3 after BLM administration but returned to the control level by day 7, and then continued to decline until day 28. Thus, *Adm* expression was strongly induced during the acute phase of the response to BLM, and there was a compensatory downregulation of AM's receptor system.

BLM-induced pulmonary injury progresses from inflammation (60). Expression of genes encoding inflammation-related factors, such as IL-6 (*Il-6*) and monocyte chemoattractant protein 1 (MCP-1) (*Ccl2*), peaked on day 3 after BLM administration then gradually decreased until day 28, suggesting that marked inflammation was induced during the acute phase and then gradually disappeared (Supplementary Figure 2E and 2F) (37). Expression of the gene encoding α-SMA (*Acta2*), a myofibroblast marker, as well as the fibrosis-related factors fibronectin and type I collagen α1 (*Fn1*, *Col1a1*) peaked on day 14 after BLM administration but had decreased by day 28. In addition, expression of the gene encoding osteopontin (*Spp1*), which is related to both inflammation and fibrosis, was elevated on days 7 and 14 and had decreased slightly, but remained elevated, on day 28 (Supplementary Figure 2G-2J) (37). These results indicate that a strong fibrotic response occurred during the later phase, beginning 14 days after BLM administration.

The pathological changes in the lungs after BLM administration were then examined (Supplementary Figure 3A) (37). Modified Ashcroft scores, which indicate the severity of pulmonary fibrosis, and the fibrotic area peaked on day 14 after BLM administration (Supplementary Figure 3B and 3C) (37). The area positive for α-SMA-immunostaining was largest on day 14, which was temporally consistent with the change in its gene expression (Supplementary Figure 3D) (37). By contrast, the numbers of CD45-positive leukocytes (Supplementary Figure 3E) (37), CD3-positive T cells (Supplementary Figure 3F) (37), and F4/80-positive macrophages (Supplementary Figure 3G) (37) peaked on day 7. These pathological findings are consistent with the gene expression results and indicate a strong inflammatory response during the acute phase after BLM administration (days 3 to 7) and a strong fibrotic response during the later phase (days 14 to 28).

Pulmonary Fibrosis Is Exacerbated in Both AM+/- and RAMP2+/- Mice

To determine the pathophysiological significance of endogenous AM in pulmonary fibrosis, we compared BLM-induced pulmonary fibrosis between AM knockout (AM+/-) mice and their wild-type (WT) littermates. Although there was no significant difference in survival after BLM administration, AM+/- mice tended to have a lower survival rate than WT mice over time (Supplementary Figure 4) (37). Lung weights increased over time in both groups but were significantly greater in AM+/- than WT mice on days 14 and 28 (Fig. 1A-1C). To quantify the amount of collagen in the lung tissues, hydroxyproline levels were measured and were found to be significantly higher in AM+/- than in WT mice on day 14 (Fig. 1D).

Gene expression analysis showed that *Il-6* expression was significantly higher in AM+/- than in WT mice during the earlier phase after BLM administration (day 3) (Fig. 1E), and *Ccl2* expression also tended to be upregulated (Fig. 1F). By contrast, *Acta2* expression was significantly higher in AM+/- than in WT mice on day 14 after BLM administration (Fig. 1J), as was *Spp1* on day 28, and *Col1a1* and *Fn1* on days 14 and 28 (Fig. 1G-I) after BLM administration. Pathological analysis showed that AM+/- lungs exhibited significantly increased inflammatory cell infiltration during the acute phase (Fig. 2B, 2F-2H) and significantly increased fibrosis and α-SMA expression during the chronic phase (Fig. 2A, 2C-2E).

Because the pathological findings showed increased infiltration by inflammatory cells during the acute phase in AM+/- lungs, we performed a FACS analysis to quantitatively evaluate each leukocyte fraction (Fig. 3A-3C). When the inflammatory cell infiltration was followed over time, it was observed that the numbers of eosinophils, monocytes and neutrophils were significantly higher in AM+/- than in WT mice during the acute phase after BLM administration (Fig. 3D). These findings indicate that endogenous AM suppresses inflammation during the acute phase and fibrosis during the chronic phase after BLM administration.

RAMP2 is highly expressed in the lung. We previously showed that the anti-inflammatory and antifibrotic effects of AM are mainly regulated by RAMP2 and that endothelial cell–specific RAMP2 knockout leads to strong inflammatory cell infiltration around blood vessels and progression to organ fibrosis with aging (61). To clarify whether the suppressive effect of endogenous AM on pulmonary fibrosis is mediated by RAMP2, BLM-induced fibrosis was compared between RAMP2 knockout (RAMP2+/-) mice and their WT littermates. The results were nearly identical to those obtained with AM+/- mice. That is, RAMP2+/- mice had heavier lung weights (Supplementary Figure 5A-5C) (37) and higher hydroxyproline contents (Supplementary Figure 5D) (37) than WT mice. In addition, gene expression of inflammatory cytokines was upregulated during the acute phase (Supplementary Figure 5E and 5F) (37), while

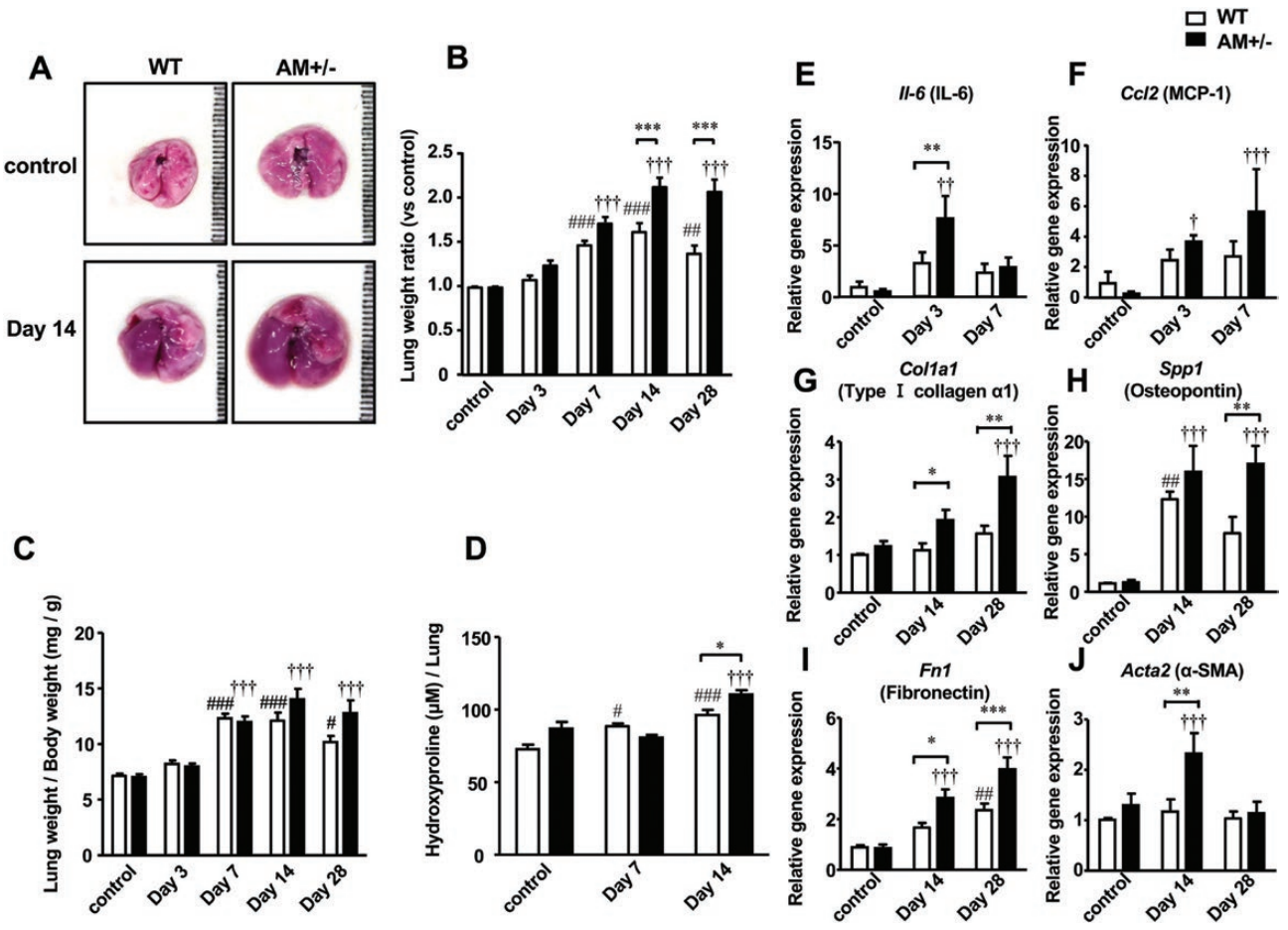

Figure 1. Bleomycin-induced pulmonary fibrosis is more severe in AM+/- mice. **A,** Appearance of the lungs from control and bleomycin-administered AM+/- and WT mice (Day 14). **B,** Lung weight ratios. The mean of the WT control group was assigned a value of 1 (n = 6-14). **C,** Lung weight / body weight (mg/g) ratios (n = 6–14). **D,** Hydroxyproline levels in the lungs of AM+/- and WT mice (n = 5). **E, F,** Quantitative real-time PCR analysis of inflammation-related genes (n = 5). **G-J,** Quantitative real-time PCR analysis of fibrosis-related genes (n = 5-6). In **E-J,** the means of the WT control groups were assigned a value of 1. Bars are means ± SEM. "*" indicates comparison between the groups, "#" indicates comparison with WT control, "†" indicates comparison with AM+/- control. *P* values were calculated using 2-way ANOVA with Tukey's test.

expression of fibrosis-related genes was upregulated during the chronic phase (Supplementary Figure 5G-5J) (37). Pathological findings were also similar to those of AM+/- mice, with greater inflammatory cell infiltration during the acute phase (Supplementary Figure 6B, 6F-6H) (37) and greater fibrosis during the chronic phase in RAMP2+/- than WT mice (Supplementary Figure 6A, 6C-6E) (37). These results suggest that the inhibitory effects of endogenous AM on inflammation and fibrosis are mediated mainly via the CLR-RAMP2 receptor complex.

Continuous Administration of AM Ameliorates Pulmonary Fibrosis

To assess the therapeutic effect of exogenously administered AM on pulmonary fibrosis, WT mice were administered BLM and then continuously infused with AM for 3, 7, or 14 days using an osmotic pump. With AM treatment, mice tended to have lighter lungs, although the effect was not significant (Supplementary Figure 7A-7C) (37). Gene expression analysis showed that expression of pro-inflammatory cytokines during the acute phase was suppressed in AM-treated mice (Supplementary Figure 7D and 7E) (37), as was expression of fibrosis-related factors during the chronic phase (Supplementary Figure 7F) (37). Similarly, pathological analysis showed that both inflammatory cell infiltration during the acute phase and fibrosis during the chronic phase were suppressed in AM-treated mice as compared to saline-treated mice (Supplementary Figure 8A-8H) (37). These results suggest that, like endogenous AM, exogenously administered AM suppresses the pathogenesis of pulmonary fibrosis and that continuous administration of AM would be an effective mean of treating pulmonary fibrosis.

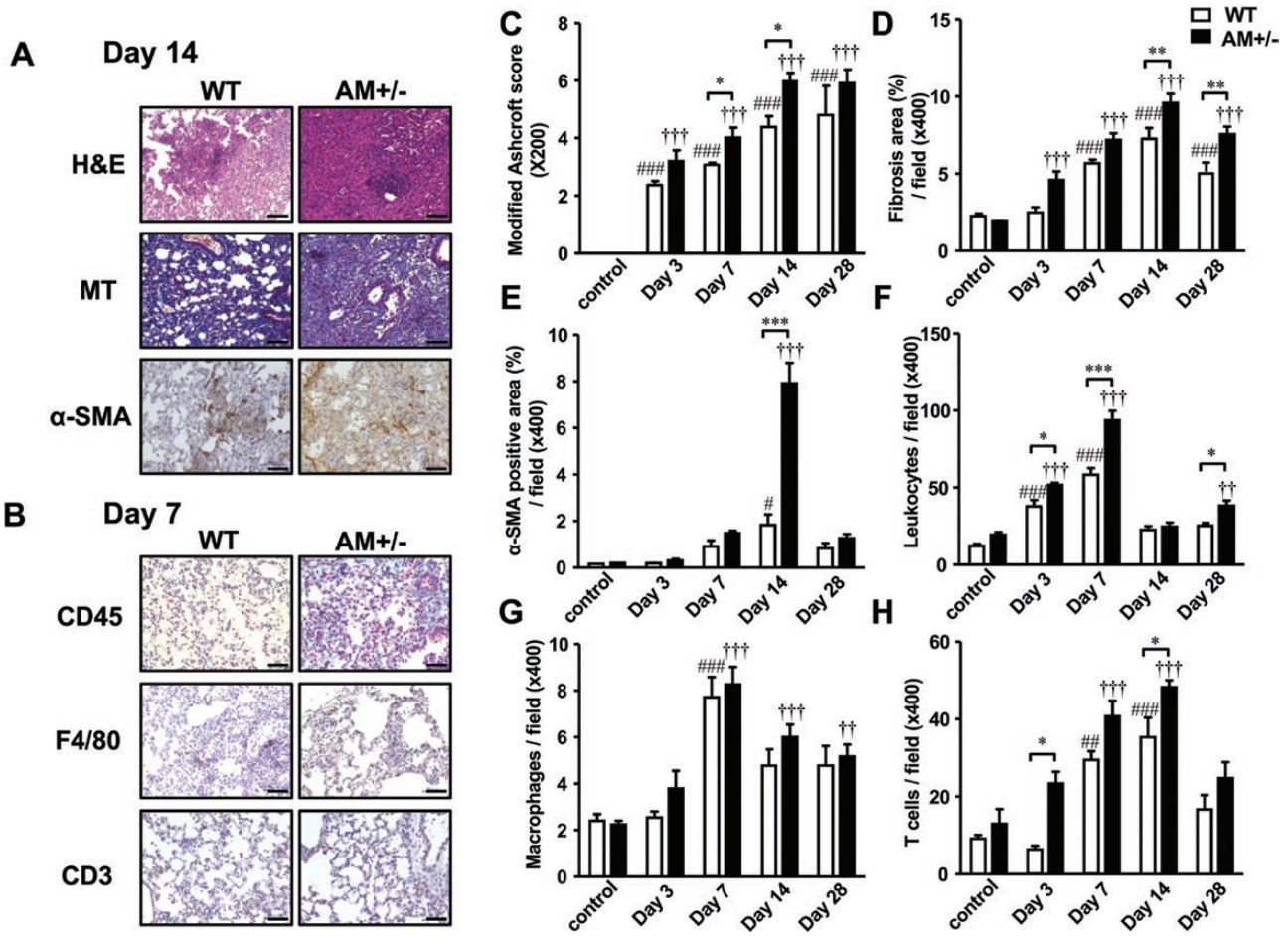

Figure 2. Pathology of bleomycin-induced inflammation and fibrosis in lungs of AM+/- mice. **A, B,** Representative photomicrographs of lung tissues stained with hematoxylin / eosin (H&E) or Masson's trichrome (MT) or immunostained for α-smooth muscle actin (α-SMA) on day 14 after bleomycin treatment (**A**) and immunostaining for CD45, F4/80 or CD3 on day 7 after bleomycin treatment (**B**). **Left column:** WT lungs, **Right column:** AM+/- lungs. Scale bars with H&E and MT staining = 100 μm. Scale bars with α-SMA, CD45, F4/80, and CD3 immunostaining = 50 μm. **C,** Modified Ashcroft score quantifying pulmonary fibrosis (n = 5-9). **D,** Percentage of the Masson's trichrome stained fibrotic area / HPF (400×) (n = 5). **E,** Percentage of α-SMA-positive area / HPF (400×) (n = 5-9). **F-H**: Numbers of CD45-positve leukocytes (**F**), F4/80-positive macrophages (**G**) and CD3-positive T cells (**H**) / HPF (400×) (n = 4-11). Bars are means ± SEM. "*" indicates comparison between the groups, "#" indicates comparison with WT control, "†" indicates comparison with AM+/- control. *P* values were calculated using 2-way ANOVA with Tukey's test.

TGF-β-Signaling is Enhanced During Pulmonary Fibrosis in AM+/- Mice

Earlier studies indicate that the transforming growth factor-β (TGF-β)-Smads pathway is involved in the process by which BLM induces pulmonary fibrosis (19, 62, 63). To explore the mechanism of the antifibrotic effect of AM, we focused on TGF-β and its intracellular signaling during the chronic phase (days 14 and 28) after BLM administration. The lungs of BLM-administered mice showed increased expression of *Tgfb1*, the gene encoding TGF-β1, but there was no significant difference between AM+/- and WT mice (Fig. 4A). On the other hand, activation of Smad3, a downstream mediator of TGF-β1 signaling, was significantly enhanced in AM+/- lungs on days 14 and 28 after BLM administration (Fig. 4B). Similarly, activation of Smad2 also tended to be upregulated in AM+/- mice, although the effect was not significantly different from that in WT mice (Fig. 4C).

Stimulation of AM+/- Fibroblasts With TGF-β Results in the Appearance of Larger Myofibroblasts

We next examined the effects of TGF-β on primary cultures of fibroblasts collected from the lungs of AM+/- and WT mice that had not been administered BLM. Figure 5A shows the results of immunostaining the primary lung fibroblasts. We also quantified the α-SMA-positive cell fraction (Fig. 5B) and measured their size (Fig. 5C). In Fig. 5B, the ratio of α-SMA-positive to vimentin-positive cells (α-SMA/vimentin) indicates the percentage of myofibroblasts among the primary mesenchymal

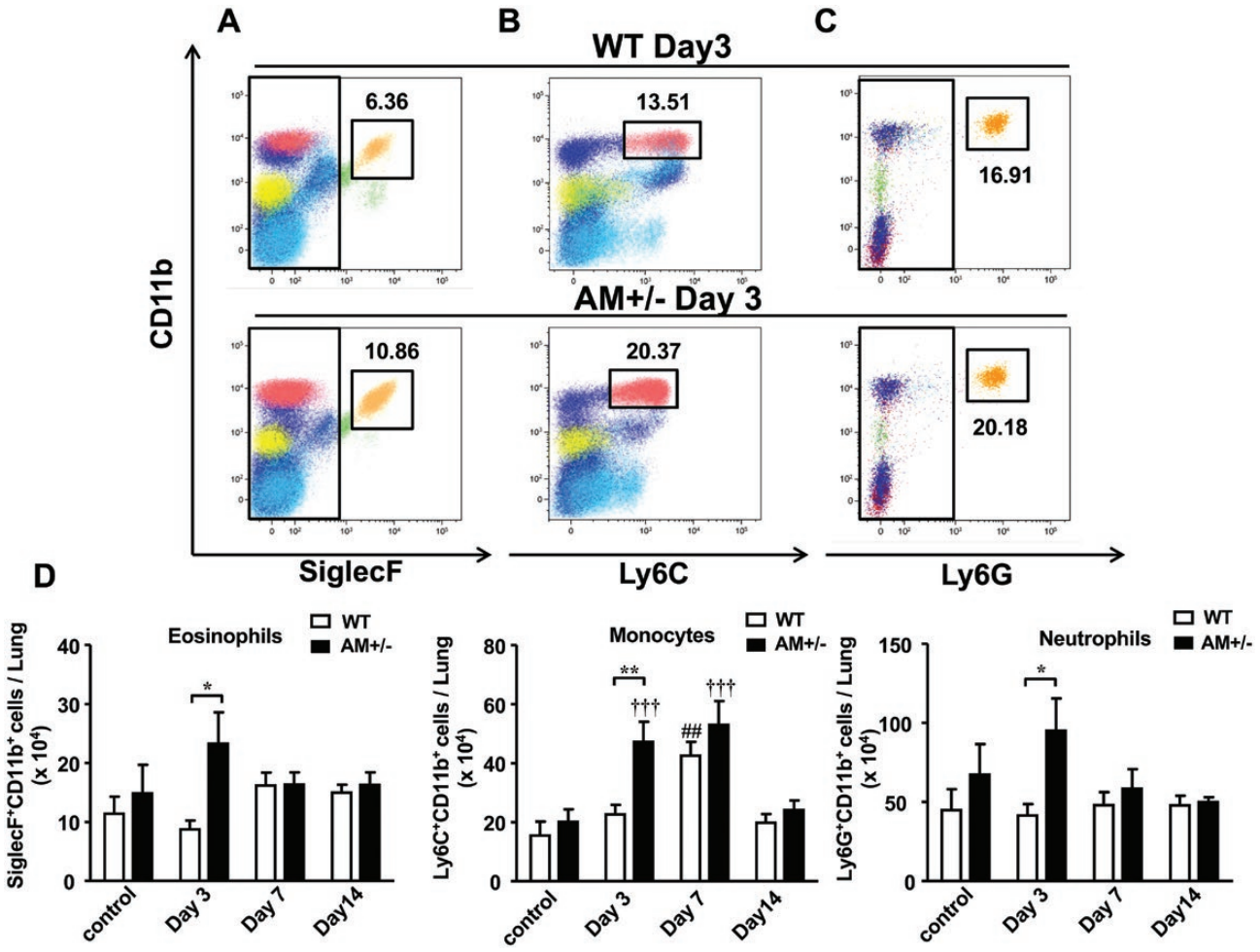

Figure 3. Changes of inflammatory cell populations during bleomycin-induced pulmonary fibrosis in AM+/- mice. **A-C,** Flow cytometric analysis of lung inflammation in AM+/- and WT mice after treatment with bleomycin. **A,** Eosinophils (SiglecF+CD11b+ in CD45+CD11c–Ly6G–). **B,** Monocytes (Ly6C+CD11b+ in CD45+CD11c–Ly6G–SiglecF–). **C,** Neutrophils (Ly6G+CD11b+ in CD45+CD11c–). Numbers indicate the percentage of the cell population in each plot. Gating was performed as shown in Supplementary Figure 1. **D,** Absolute numbers of eosinophils, monocytes and neutrophils in lungs from mice left untreated or treated with bleomycin (n = 4–6). Bars are means ± SEM. "*" indicates comparison between the groups, "#" indicates with comparison with WT control, "†" indicates comparison with AM+/- control. *P* values were calculated using 2-way ANOVA with Tukey's test.

cells (mostly fibroblasts). Compared with WT, cells cultured from AM+/- lungs tended to have a higher proportion of myofibroblasts that were positive for α-SMA immunostaining (Fig. 5B, control). In addition, α-SMA-positive myofibroblasts from AM+/- lungs tended to be larger in size, even when unstimulated (Fig. 5C, control). Among the cells from WT lungs, the number of α-SMA-positive myofibroblasts increased after TGF-β-stimulation, although the change was not significant (Fig. 5B, compare the white columns between control and TGF-β1). These cells also tended to be enlarged (Fig. 5C, compare the white columns between control and TGF-β1). Among the cells from AM+/- lungs, the increase in α-SMA-positive cells (Fig. 5B, compare the black columns between control and TGF-β1) and their cellular enlargement (Fig. 5C, compare the black columns between control and TGF-β1) were made much more pronounced by TGF-β stimulation. Notably, however, the TGF-β-induced changes observed in AM+/- cells were canceled by application of AM to the cells (Fig. 5B and Fig. 5C, compare the black columns between TGF-β1 and TGF-β1+AM). These results indicate that under conditions where AM levels are decreased while TGF-β levels are increased, the numbers of α-SMA-positive myofibroblasts are increased and the cells are larger.

Comparison of the proliferative and migratory capacities of TGF-β-stimulated AM+/- and WT cells revealed that the proliferative capacity of AM+/- cells was significantly lower than that of WT cells (Fig. 6A). Likewise, scratch assays showed that AM+/- cells had a significantly lower migratory capacity than WT cells (Fig. 6B). These results suggest that when fibroblasts derived from the lungs of AM+/- mice are stimulated with TGF-β, they likely differentiate into myofibroblasts characterized

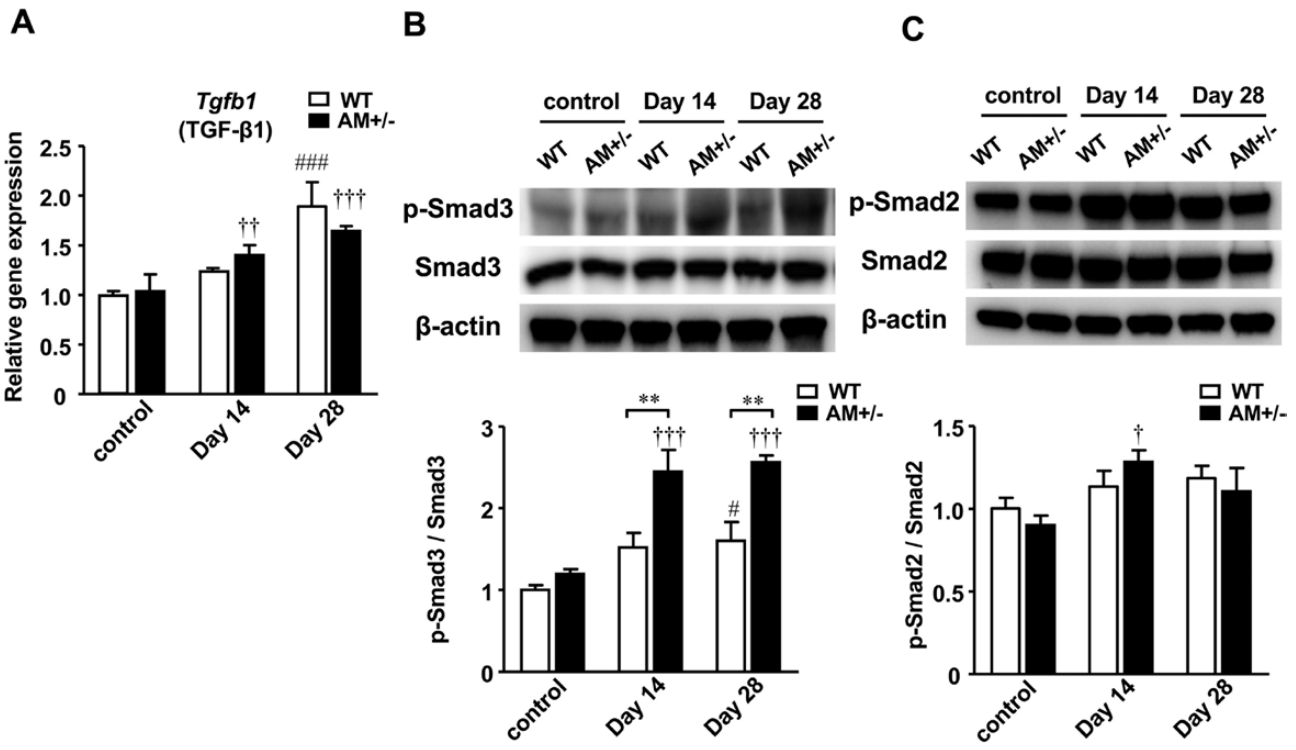

Figure 4. TGF-β-signaling is enhanced in bleomycin-administered AM+/- mice. **A,** Quantitative real-time PCR analysis of *Tgfb1* expression 14 and 28 days after bleomycin administration to AM+/- and WT mice. The mean of the WT control was assigned a value of 1 (n = 5). Bars are means ± SEM. **B, C, Upper row:** Representative Western blots of Smad3 and p-Smad3 (**B**) and Smad2 and p-Smad2 (**C**) in AM+/- and WT lungs left untreated (control) and on days 14 and 28 after bleomycin administration. β-actin was used as a loading control. **B, C, Lower row:** Levels of Smad2 and Smad3 activation as indicated by band intensity ratios (p-Smad2 / Smad2 and p-Smad3 / Smad3) Means of WT controls were assigned a value of 1 (n = 3-4). Bars are means ± SEM. "*" indicates compared between the groups, "#" indicates comparison with WT control, "†" indicates comparison with AM+/- control. *P* values were calculated using 2-way ANOVA with Tukey's test.

by larger size and lower proliferative and migratory capacities.

Stimulation of AM+/- Fibroblasts With TGF-β Increases Nonproliferating Myofibroblasts

Given the findings summarized in the previous section, we classified lung-derived cells based on their intracellular actin fiber formation, the presence or absence of α-SMA expression, and their proliferation potential in addition to their morphology. As described previously (64), fluorescence microscopy was used to classify the cells into 4 types based on their actin fiber formation (phalloidin staining), α-SMA expression, and proliferative potential (Ki-67 immunostaining) (Fig. 7). Cells with mild actin fiber formation, no expression of α-SMA, and high proliferative potential were classified as fibroblasts (Fbs). Cells with actin fiber formation but no expression of α-SMA and high proliferative potential were classified as proto-myofibroblasts (proto-MyoFbs). Cells with high proliferative potential and both actin fiber formation and α-SMA expression were classified as proliferating myofibroblasts (p-MyoFbs). And cells with actin fiber formation and α-SMA expression but without proliferative capacity were classified as nonproliferating myofibroblasts (non-p-MyoFbs) (Fig. 7). Cells that could not be classified based on immunostaining were excluded from the counting; about 70% to 80% of the cells examined were classified into these 4 types. Figure 8 shows the Fb (Fig. 8A), proto-MyoFb (Fig. 8B), p-MyoFb (Fig. 8C), and non-p-MyoFb (Fig. 8D) fractions expressed as percentages of the total classified cells. Only after stimulation with TGF-β1 were there significant differences in the percentages of each cell type between AM+/--derived and WT-derived cells. In other words, TGF-β1 stimulation of AM+/- lung-derived fibroblasts led to a decrease in cells classified as p-MyoFbs (Fig. 8C) and an increase in cells classified as non-p-MyoFbs (Fig. 8D). On the other hand, the change in cell profile (decrease of p-MyoFbs and increase of non-p-MyoFbs) observed among TGF-β1-stimulated AM+/- derived cells was blocked when AM was applied to the cells (Fig. 8C and 8D, TGF-β1 + AM).

We also immunostained AM+/- and WT lung specimens to determine how the cell profiles had changed within the lung 14 days after BLM administration. The results showed that numbers of p-MyoFbs

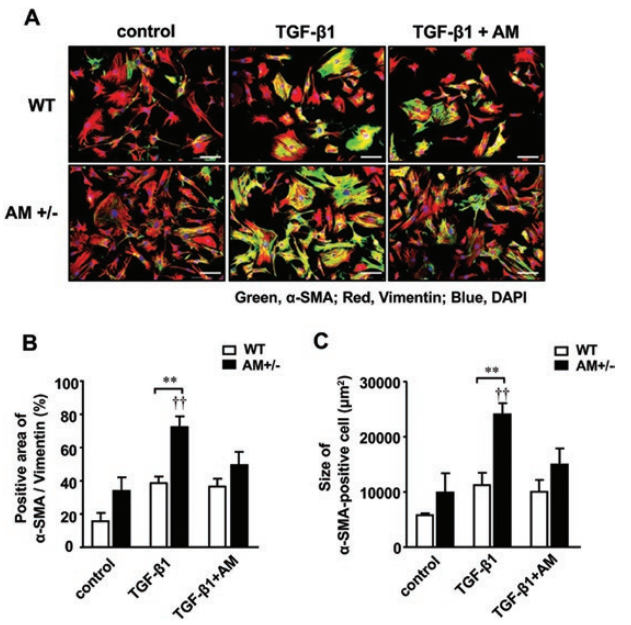

Figure 5. TGF-β1-induced differentiation of fibroblasts to myofibroblasts and its suppression by AM. **A,** Representative images of immunostained (Green: α-SMA, Red: vimentin, Blue: DAPI) primary cultured fibroblasts isolated from the lungs of AM+/- and WT mice. Cells were grown to 70% confluence. Immunostaining was performed in control cells and cells pretreated with AM (10^{-7} M) or PBS for 2 hours and then stimulated with TGF-β1 (10 ng/mL) for 24 hours. Scale bars = 100 μm. **B,** Percentage of α-SMA-positive area / vimentin-positive area. **C:** Size of α-SMA-positive cells (**B, C**). Data are from 3 independent experiments. Bars are means ± SEM. "*" indicates comparison between the groups, "†" indicates comparison with AM+/- control. *P* values were calculated using 2-way ANOVA with Tukey's test.

(α-SMA [+], Ki67 [+]) numbers were decreased while non-p-MyoFb (α-SMA [+], Ki67 [-]) numbers were increased in AM+/- lungs after BLM administration

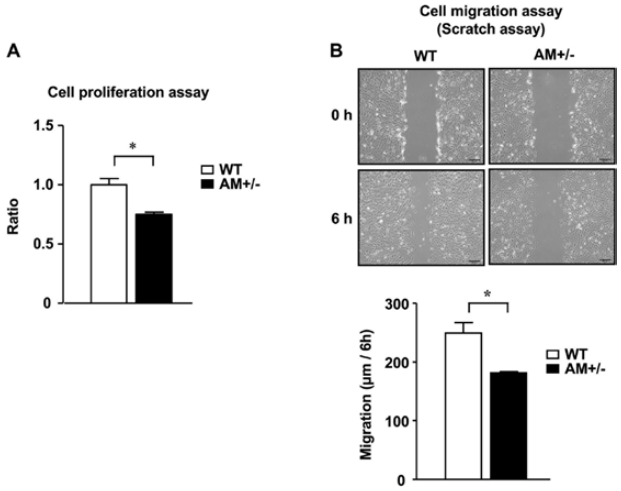

Figure 6. Cell proliferation and migration is reduced in primary cultured AM+/- lung fibroblasts stimulated with TGF-β. **A,** Cell proliferation was assessed using a cell counting kit with water-soluble tetrazolium salt as a substrate. Data are shown as the ratio of cell proliferation when the mean of the WT cells was assigned a value of 1 (n = 4). **B,** Cell migration was assessed using scratch assays. **Upper row:** Representative photomicrographs showing the status of the scratch in a cultured cell monolayer at 0 and 6 hours after scratching. Scale bars = 200 μm. **Lower row:** The cell migration distance was calculated from change in the width of the scratch between 0 and 6 hours. The data are from 3 independent experiments. Bars are means ± SEM. "*" indicates comparison between the groups. *P* values were calculated using Student's *t* test.

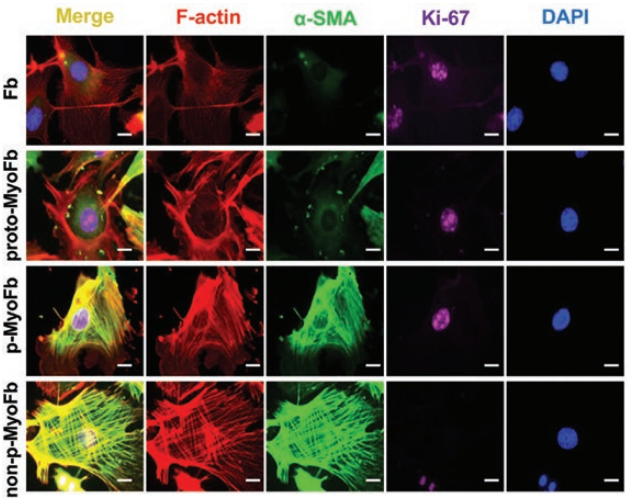

	F-actin	α-SMA	Ki-67
fibroblast (Fb)	+/−	−	+
proto-myofibroblast (proto-MyoFb)	+	−	+
proliferating-myofibroblast (p-MyoFb)	+	+	+
nonproliferating-myofibroblast (non-p-MyoFb)	+	+	−

Figure 7. Classification of the lung fibroblasts stimulated with TGF-β. Shown are phalloidin staining, DAPI staining, and immunostaining for α-SMA and Ki67 in representative cells in each indicated category. Cells with mild actin fiber formation, no expression of α-SMA, and high proliferative potential (F-actin [+/-], α-SMA [-], Ki-67 [+]) were defined as fibroblasts (Fbs). Cells with actin fiber formation but no expression of α-SMA and high proliferative capacity (F-actin [+], α-SMA [-], Ki-67 [+]) were defined as proto-myofibroblasts (proto-MyoFbs). Cells with high proliferative potential, which showed both actin fiber formation and expression of α-SMA (F-actin [+], α-SMA [+], Ki-67 [+]) were defined as proliferating myofibroblasts (p-MyoFbs). Cells with actin fiber formation and α-SMA expression but lost proliferative capacity (F-actin [+], α-SMA [+], Ki-67 [-]) were defined as nonproliferating myofibroblasts (non-p-MyoFbs). Scale bars = 20 μm.

(Supplementary Figure 9) (37), which is consistent with the in vitro study (Fig. 8).

Nonproliferating Myofibroblasts Are Highly Productive and Contractile

To further investigate the cells classified as non-p-MyoFbs, we examined the characteristics of TGF-β1-stimulated AM+/- cells. We found that expression of the genes encoding type I collagen α1 (*Col1a1*), a central component of extracellular matrix; TIMP-1 (*Timp-1*), a suppressor of collagen degradation; and MCP-1 (*Ccl2*), a chemoattractant of inflammatory cells; were all significantly upregulated in TGF-β1-stimulated AM+/- cells (Fig. 9A-9C). These changes in gene expression were canceled when AM was added. On the other hand, expression of the gene encoding Meflin (*Islr*), a recently discovered marker of steady-state fibroblasts (65, 66), was greatly reduced in both AM+/- and WT cells upon stimulation with TGF-β1 (Fig. 9D). The marked downregulation of *Islr* by TGF-β1 was not reversed when AM was added.

As the differentiated myofibroblasts exhibited higher levels of actin filaments, some of which were α-SMA-positive, we examined their ability to contract within a 3-dimensional collagen matrix (Fig. 10A). AM+/- and WT cells both contracted upon TGF-β1-stimulation, but the contractions were significantly greater in AM+/- cells (Fig. 10B, TGF-β1). These TGF-β1-induced contractions were also canceled by application of AM (Fig. 10B, TGF-β1 + AM).

Collectively, these findings indicate that non-p-MyoFbs are larger in size, have lower capacities for proliferation and migration, but higher capacities for filamentous actin formation, contraction, and production of extracellular matrix and chemoattractant for recruitment of inflammatory cells.

TGF-β Downstream Signaling Is Activated in Nonproliferating Myofibroblasts

Because TGF-β signaling was more activated in the lungs of BLM-administered AM+/- mice than WT mice, we investigated whether it was more activated in TGF-β-stimulated

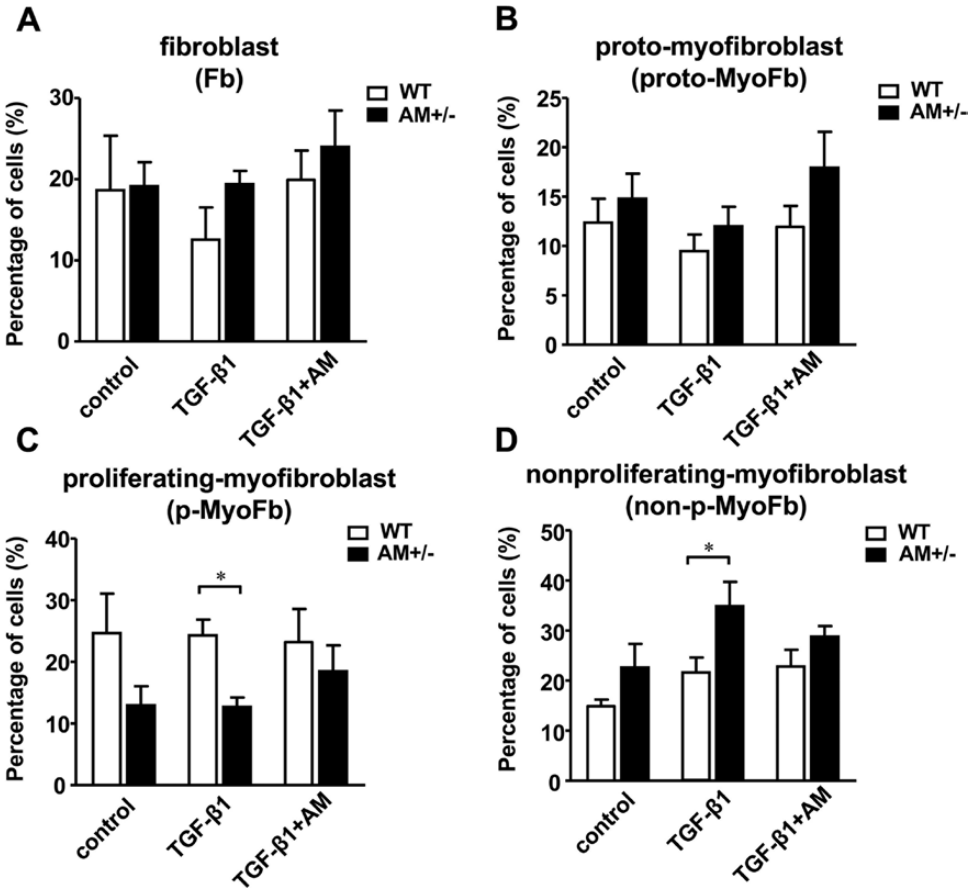

Figure 8. Stimulation of AM+/- fibroblasts with TGF-β increases nonproliferating myofibroblasts. **A-D,** AM+/- and WT lung fibroblasts were classified into 4 categories (A: fibroblasts [Fbs], B: proto-myofibroblasts [proto-MyoFbs], C: proliferating myofibroblasts [p-MyoFbs] and D: nonproliferating myofibroblasts [non-p-MyoFbs]) based on cell staining. Shown are their percentages among the control, TGF-β1-stimulated and TGF-β1-stimulated + AM groups. Data are from 3 independent experiments. Bars are means ± SEM. "*" indicates comparison between the groups. *P* values were calculated using 2-way-ANOVA with Tukey's test.

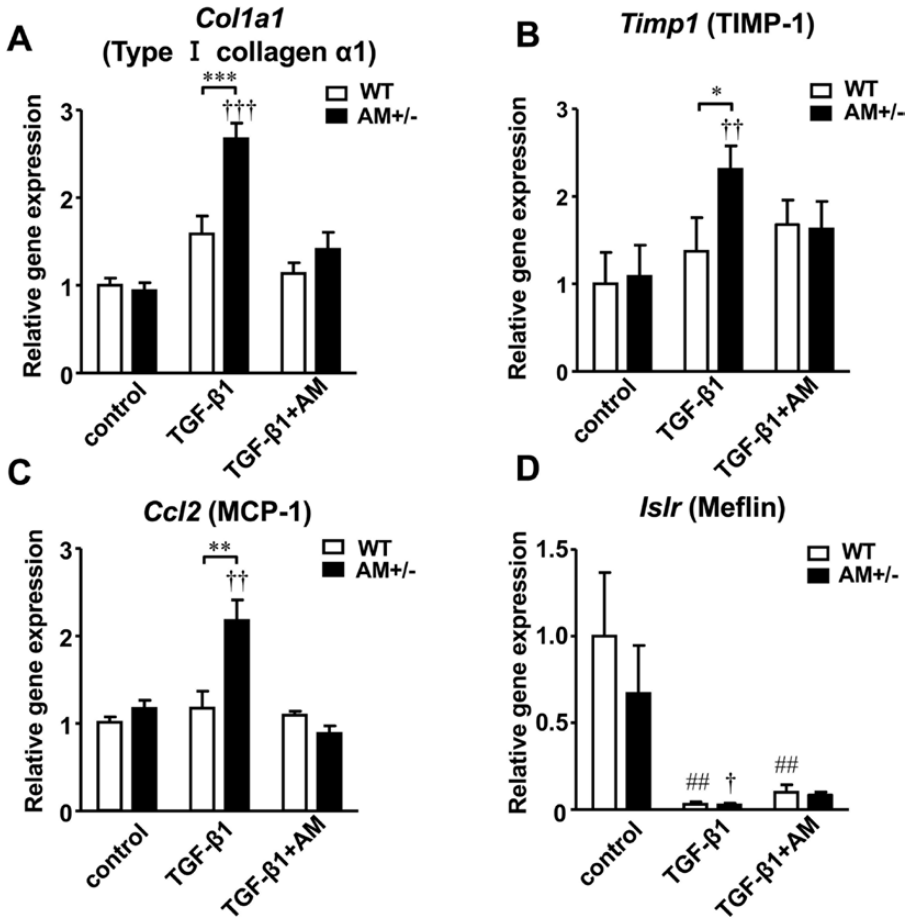

Figure 9. TGF-β-stimulated AM+/- fibroblasts show upregulation of genes related to fibrosis and inflammation but downregulation of a steady-state fibroblast marker. **A-D,** Quantitative real-time PCR analysis of *Col1a1* (Type I collagen α1) (**A**), *Timp1* (TIMP-1) (**B**), *Ccl2* (MCP-1) (**C**) and *Islr* (Meflin) (**D**) in AM+/- and WT lung fibroblasts. The means of the WT control group were assigned a value of 1 (n = 5). Bars are means ± SEM. "*" indicates comparison between the groups, "#" indicates comparison with WT control, "#" indicates comparison with WT control, "†" indicates comparison with AM+/- control. *P* values were calculated using 2-way ANOVA with Tukey's test.

AM+/- fibroblasts than WT fibroblasts. In the absence of stimulation, the activation levels of Smad2 and Smad3, two downstream TGF-β signaling molecules, did not differ between AM+/- and WT cells (Fig. 11A and 11B, control). By contrast, when stimulated with TGF-β, AM+/- cells showed a significantly greater increase in Smad3 activation than WT cells (Fig. 11A, TGF-β1), but that effect was suppressed by application of AM (Fig. 11A, TGF-β1 + AM). Smad2 activation tended to increase when AM+/- cells were stimulated with TGF-β, but the effect did not significantly differ from WT cells (Fig. 11B, TGF-β).

Those results suggest that TGF-β and its downstream signaling molecules are involved in the differentiation of AM+/- lung-derived fibroblasts into non-p-MyoFbs. To further test that idea, we examined how non-p-MyoFbs were affected by treatment with SB431542, a selective TGF-β receptor-1 (TGFβR1) inhibitor, or SIS3, a Smad3-selective inhibitor (Fig. 12A). We found that treatment with SB431542 or SIS3 reduced the increase in non-p-MyoFb seen when AM+/- cells were stimulated with TGF-β and eliminated the significant difference between AM+/- and WT cells (Fig. 12B and 12C). The effect of these TGF-β signaling inhibitors (SB431542 or SIS3) on the appearance of non-p-MyoFbs was similar to the effect of external AM seen in Fig. 5.

Smad7 Expression Is Downregulated in AM+/- Lungs and TGF-β-Stimulated AM+/- Fibroblasts After BLM Administration

Unlike Smad2 and Smad3, which are receptor-activated Smads (R-Smads), Smad7, an antagonistic Smad, stably binds to TGFβR1, thereby suppressing activation of Smad2, Smad3, and TGF-β signaling. We found that Smad7 expression was significantly downregulated in the lungs of AM+/- mice compared to WT mice, both in the controls (Fig. 13A, control) and 14 days after BLM administration (Fig. 13A, Day14). Furthermore, Smad7 expression

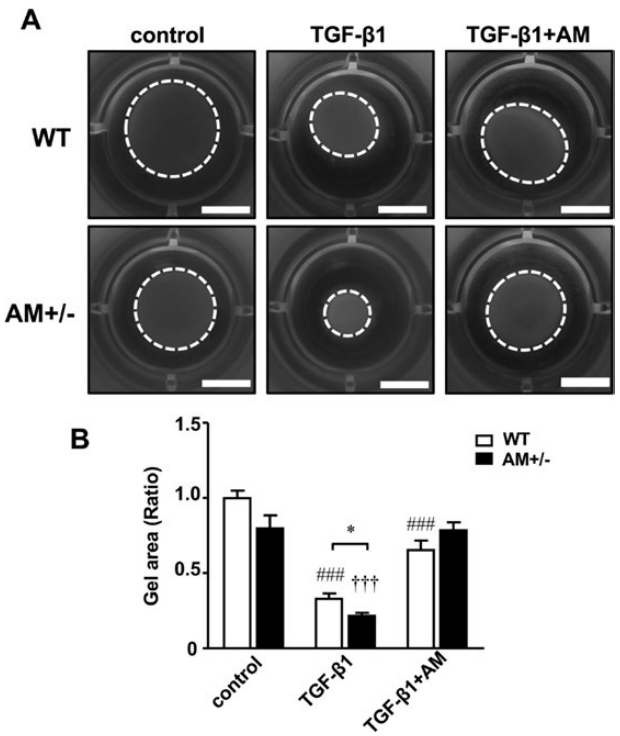

Figure 10. TGF-β-stimulated AM+/- fibroblasts show enhanced contractility. **A,** Representative images of culture dishes in a gel contraction assay. **A,** "Contracture rings" (white dotted circles) show the borders of the measured area 12 hours after gel release. Scale bars = 5 mm. **B,** Relative gel area 12 hours after collagen gel release from the well's wall. A smaller gel area indicates greater cellular contraction. The mean of the WT control group was assigned a value of 1. Data are from 3 independent experiments. Bars are means ± SEM. "*" indicates comparison between the groups, "#" indicates comparison with WT control, "†" indicates comparison with AM+/- control. *P* values were calculated using 2-way ANOVA with Tukey's test.

was also significantly downregulated in TGF-β-stimulated AM+/- cells as compared with WT cells (Fig. 13B, TGF-β). However, when AM was added, the downregulation of Smad7 was reversed (Fig. 13B, TGF-β+AM). In addition, treating WT cells with AM alone significantly upregulated Smad7 expression (Fig. 13C), which may in turn suppress TGF-β-Smad3 signaling.

miR-21 Expression Was Upregulated in BLM-Administered AM+/- Lungs and TGF-β-Stimulated AM+/- Fibroblasts

It is now apparent that microRNAs are involved in a wide variety of pathophysiological processes, including pulmonary fibrosis. Among them, we focused on the pro-fibrotic miR-21, encoded by *Mir21* (67). In control lungs, there was no difference in the expression of miR-21 between AM+/- and WT mice (Fig. 14A, control). However, BLM administration resulted in a significant elevation in miR-21 expression in AM+/- mice on day 14 (Fig. 14A, Day 14). WT mice also showed the tendency toward elevated miR-21 expression after BLM administration, but the effect was not statistically significant. As a result, miR-21 expression significantly differed between AM+/- and WT mice on day 14 (Fig. 14A, Day14). The upregulated miR-21 expression declined to control levels by day 28 (Fig. 14A, Day 28).

To confirm whether miR-21 expression is related to myofibroblast differentiation, we also examined its expression in the fibroblasts derived from AM+/- and WT lungs and compared its expression with and without TGF-β and AM administration (Fig. 14B). In the absence of TGF-β1, miR-21 expression did not differ between AM+/- and WT cells with or without AM administration (Fig. 14B, TGF-β1[-]). By contrast, upon stimulation with TGF-β1, miR-21 expression was upregulated to a significantly greater degree in AM+/- cells than WT cells (Fig. 14B, TGF-β1[+], AM[-]). When AM was added in addition to TGF-β1, the difference in miR-21 expression between AM+/- and WT cells was eliminated (Fig. 14B, TGF-β1[+], AM[+]). Taken together, these results suggest that (1) administering BLM to WT mice or stimulating WT cells with TGF-β1 elicit only small, nonsignificant changes in miR-21 expression; (2) miR-21 expression in both AM+/- and WT cells is unaffected by AM alone; and (3) only BLM-administered AM+/- mice and TGF-β1-stimulated AM+/- cells show significant upregulation of miR-21 expression. Thus, miR-21 is significantly upregulated in myofibroblasts only when TGF-β levels are increased with a simultaneous decrease in AM levels.

Downregulation of miR-21 in TGF-β-Stimulated AM+/- Cells Suppresses the Differentiation of Nonproliferating Myofibroblasts

To confirm the involvement of miR-21 in the differentiation of non-p-MyoFbs, we next assessed the effect of a miR-21 inhibitor on the differentiation of TGF-β-stimulated AM+/- and WT fibroblasts (Fig. 15). Application of the miR-21 inhibitor to the cells significantly reduced the number of large α-SMA-positive myofibroblasts (ie., non-p-MyoFbs among AM+/-). These results indicate that miR-21 is a regulator of non-p-MyoFb differentiation through activation of TGF-β signaling in AM+/- cells.

Discussion

In the present study, we used a mouse BLM-induced pulmonary fibrosis model to investigate the pathophysiological significance of the AM-RAMP2 system. We found that pulmonary fibrosis was exacerbated in both AM+/- and RAMP2+/- mice as compared with WT mice. Consistent with that finding, both AM+/- and RAMP2+/- mice

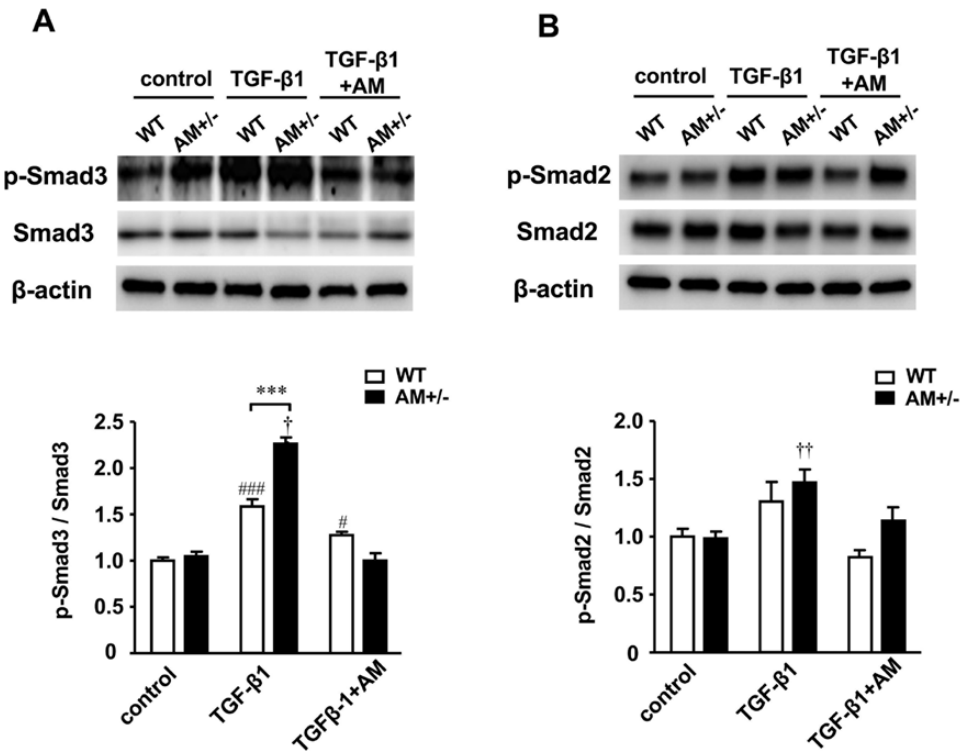

Figure 11. TGF-β-stimulated AM+/- fibroblasts show greater Smad3 activation. **A, B, Upper row**: Representative Western blots showing expression of Smad3 and phosphorylated (p)-Smad3 (**A**) and Smad2 and p-Smad2 (**B**) in AM+/- and WT lung fibroblasts (control and TGF-β1-stimulated cells with or without AM treatment). β-actin was used as a loading control. **A, B, Lower row:** p-Smad3 / Smad3 (**A**) and p-Smad2 /Smad2 (**B**) band density ratios showing the level of Smad3 (**A**) and Smad2 (**B**) activation. Means of WT controls were assigned a value of 1. Data are from 4 independent experiments. Bars are means ± SEM. "*" indicates comparison between the groups, "#" indicates comparison with WT control, "†" indicates comparison with AM+/- control. *P* values were calculated using 2-way ANOVA with Tukey's test.

exhibited marked pulmonary inflammation during the acute phase after BLM administration, which was followed by fibrosis during the chronic phase. Kach et al reported that transgenic mice overexpressing RAMP2 under the control of the α-SMA promoter had improved survival and reduced pulmonary fibrosis in the BLM model (41). Their results mirror those of our AM+/- and RAMP2+/- mice and support the idea that the AM-RAMP2 system acts as an inhibitory mediator in the pathogenesis of pulmonary fibrosis.

The TGF-β-Smads pathway is known to be a major cause of fibrosis. Within the lungs of AM+/- mice administered BLM, the activation level of Smad3, a receptor-activated Smad, was increased. Also increased was expression of *Tgfb1*, the gene encoding TGF-β1, though the expression level did not significantly differ between WT and AM+/- mice. These observations suggest that in AM+/- mice, BLM administration does not increase *Tgfb1* expression itself, but instead enhances the activation of downstream mediators of TGF-β. On the other hand, activation of Smad2, another receptor-activated Smad, was not significantly changed in AM+/- as compared with WT mice. Although the structure of Smad2 is highly similar to that of Smad3, and both Smad2 and Smad3 are directly phosphorylated by TGFβR1, a receptor tyrosine kinase, they do not share similar DNA-binding activity (68). Gu et al reported that it is Smad3, not Smad2, that functions as the major mediator of TGF-β1 signaling to activate *Acta2* (α-SMA) gene expression in vitro (69). That result was confirmed in Smad3 knockout mice, which showed attenuated lung fibrosis after BLM administration (68). In the present study, we also found a clear and significant difference in the levels of Smad3 activation between AM+/- and WT cells after TGF-β stimulation. These observations suggest that TGFβR1 and Smad3 activation are important downstream TGF-β signals involved in exacerbating pulmonary fibrosis in AM+/- mice. This was also confirmed by the experiments using a TGFβR1 or Smad3 inhibitor, both of which suppressed the effect of TGF-β.

Fibroblasts are the major mesenchymal cell type in the lungs, and differentiation from fibroblasts to myofibroblasts is a key event in the process of fibrosis (70). When inflammatory stimuli persist, fibroblasts differentiate into myofibroblasts, which exhibit enhanced extracellular matrix production. The resultant acceleration of extracellular matrix deposition leads to the development of fibrosis (43). TGF-β is a potent inducer of differentiation to α-SMA-positive myofibroblasts (MyoFbs) (71). In the

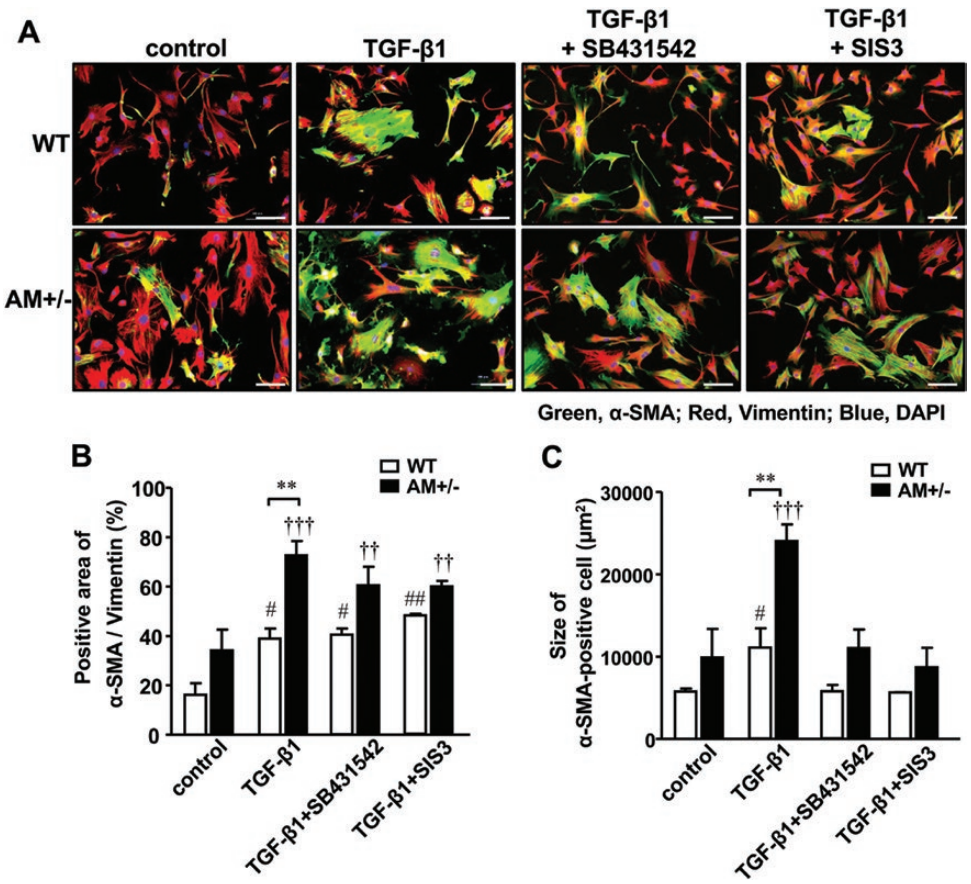

Figure 12. TGFβRI or Smad3 inhibition suppresses the occurrence of nonproliferating myofibroblasts (non-p-MyoFbs) among TGF-β-stimulated AM+/- fibroblasts. **A,** Representative images of immunostained (Green: α-SMA, Red: vimentin, Blue: DAPI) primary cultured lung fibroblasts isolated from AM+/- and WT mice. The cells were grown to 70% confluence. Immunostaining was performed in control cells and in cells stimulated with TGF-β1 (10 ng/mL) for 24 hours with or without SB431542 (10 μM), an inhibitor of TGF-β type I receptor (TGFβRI) or SIS3 (3 μM), an inhibitor of Smad3. Scale bars = 100 μm. **B,** Percentage α-SMA-positive area/vimentin-positive area. **C,** Size of α-SMA-positive cells. Data are from 3 independent experiments. Bars are means ± SEM. "*" indicates comparison between the groups, "#" indicates comparison with WT control, "†" indicates comparison with AM+/- control. *P* values were calculated using 2-way ANOVA with Tukey's test.

present study, TGF-β-stimulated α-SMA-positive MyoFbs derived from AM+/- mice showed reduced proliferative and migratory potential. These cells were also larger in size and exhibited enhanced contractility. Driesen et al reported that TGF-β promotes differentiation of proliferating MyoFbs (p-MyoFbs) to MyoFbs that exhibit a near absence of proliferation, and they named them nonproliferating-MyoFbs (non-p-MyoFbs) (72). Non-p-MyoFbs produce large amounts of collagen and chemoattractant molecules that recruit inflammatory cells. We also observed that TGF-β-stimulated AM+/- cells exhibited higher expression of collagen, TIMP1, and MCP-1 than WT cells. TIMP1 inhibits degradation of extracellular matrix by inactivating matrix metalloproteinases. MCP-1 acts as a migratory factor for monocytes and is associated with chronic inflammation. These results suggest that non-p-MyoFbs, which were increased among TGF-β-stimulated AM+/- cells, are deeply involved in the exacerbation of pulmonary fibrosis. These properties of non-p-MyoFbs were suppressed by adding AM to TGF-β-stimulated AM+/- cells. By contrast, expression of Meflin, a recently discovered marker of steady-state fibroblasts (65, 66), was downregulated by the TGF-β stimulation, but that effect was not reversed by AM treatment. This suggests that AM can suppress TGF-β-induced differentiation of p-MyoFbs to non-p-MyoFbs, but it cannot return them to normal steady-state fibroblasts.

It is now clear that dysregulation of microRNAs is linked to a wide variety of diseases, including fibrosis of the liver (73), kidney (74), heart (75), and lung (67). MicroRNAs work as regulators of gene expression, and some have also attracted attention as regulators of the TGF-β-Smads pathway and fibrosis (67). Among them, we focused on miR-21, encoded by *Mir21*, levels of which are reportedly elevated in the lungs of pulmonary fibrosis patients and BLM-administered mice (76). Moreover, the enhanced *Mir21* expression is primarily localized in myofibroblasts, where its product, miR-21, activates them to promote the progression of fibrosis (76). The profibrotic properties of

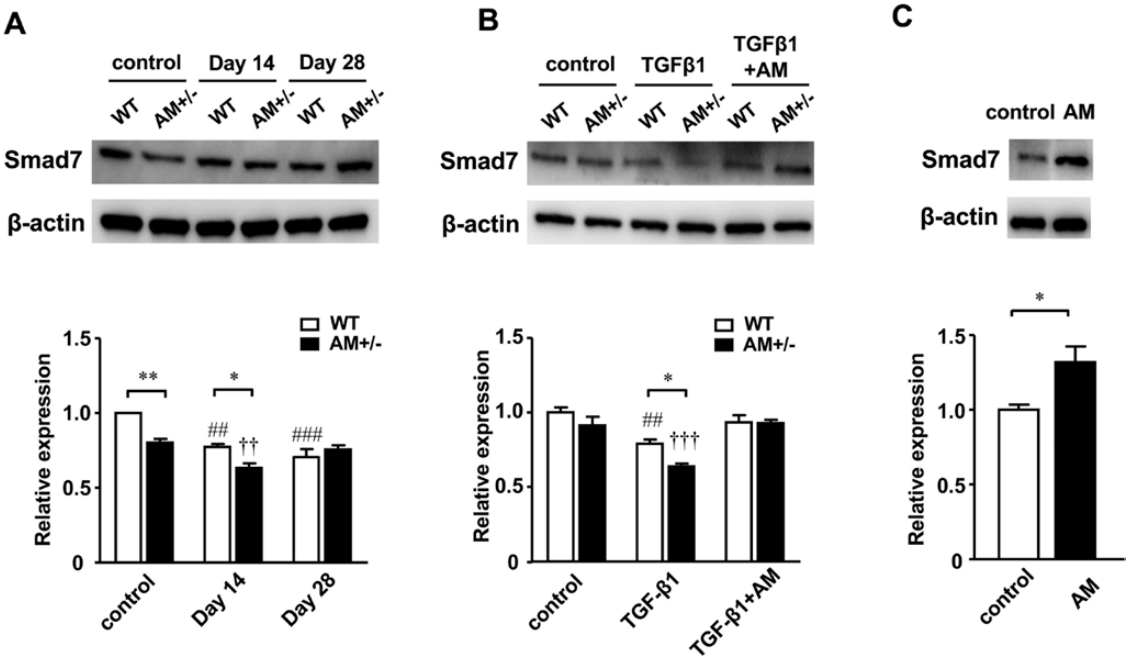

Figure 13. Expression of Smad7 is downregulated in AM+/- but is restored by AM treatment. **A, B, Upper row:** Representative Western blots showing expression of Smad7 in lungs from AM+/- and WT mice left untreated (control) and 14 and 28 days after bleomycin administration (**A**) and in AM+/- and WT lung fibroblasts (control cells and TGF-β1-stimulated cells with or without AM treatment) (**B**). β-actin was used as a loading control. **A, B, Lower row:** Relative levels of Smad7 expression determined from the corresponding band densities. The means of the WT controls were assigned a value of 1 (n = 3–4). Bars are means ± SEM. "*" indicate comparison between the groups, "#" indicates comparison with WT control, "†" indicates comparison with AM+/- control. *P* values were calculated using 2-way ANOVA with Tukey's test. **C, Upper row:** Representative Western blots showing expression of Smad7 in WT lung fibroblasts with or without 10^{-7} M AM for 24 hours. β-actin was used as a loading control. **C, Lower row:** Relative levels of Smad7 expression determined from the corresponding band densities. The mean of the WT control was assigned a value of 1 (n = 3). Bars are means ± SEM. "*" indicates comparison between the groups. *P* value was calculated using Student's *t* test.

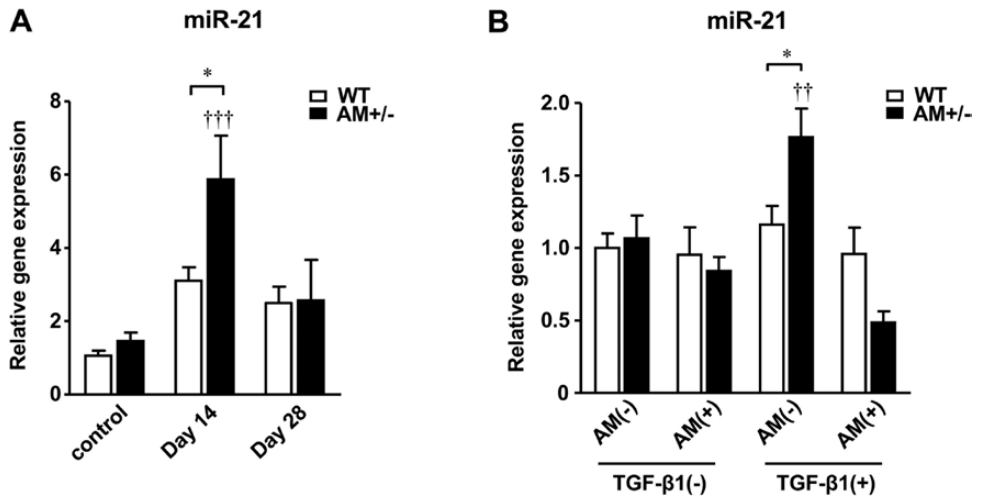

Figure 14. Expression of miR-21 is upregulated in bleomycin-administered AM+/- mice and TGF-β-stimulated AM+/- fibroblasts. **A,** Quantitative real-time PCR analysis of microRNA-21 (miR-21) in AM+/- and WT mice left untreated (control) and 14 and 28 days after bleomycin administration. The mean of the WT control was assigned a value of 1 (n = 5). Bars are means ± SEM. "*" indicates comparison between the groups, "†" indicates comparison with AM+/- control. **B,** Quantitative real-time PCR analysis of miR-21 in AM+/- and WT lung fibroblasts. The mean of the WT control (TGF-β [-], AM [-]) group was assigned a value of 1 (n = 5). Bars are means ± SEM. "*" indicates comparison between the groups, "†" indicates comparison with AM+/- control (TGF-β [-], AM [-]). *P* values were calculated using 2-way ANOVA with Tukey's test.

miR-21 are thought to be mediated via downregulation of Smad7, an inhibitor of the TGF-β-Smads pathway. Indeed, Smad7 is reported to be a direct target of miR-21 in various diseases including pulmonary fibrosis, renal fibrosis, and cancers (67, 74, 77). In the present study, we were able to confirm that *Mir21* expression is upregulated, while Smad7

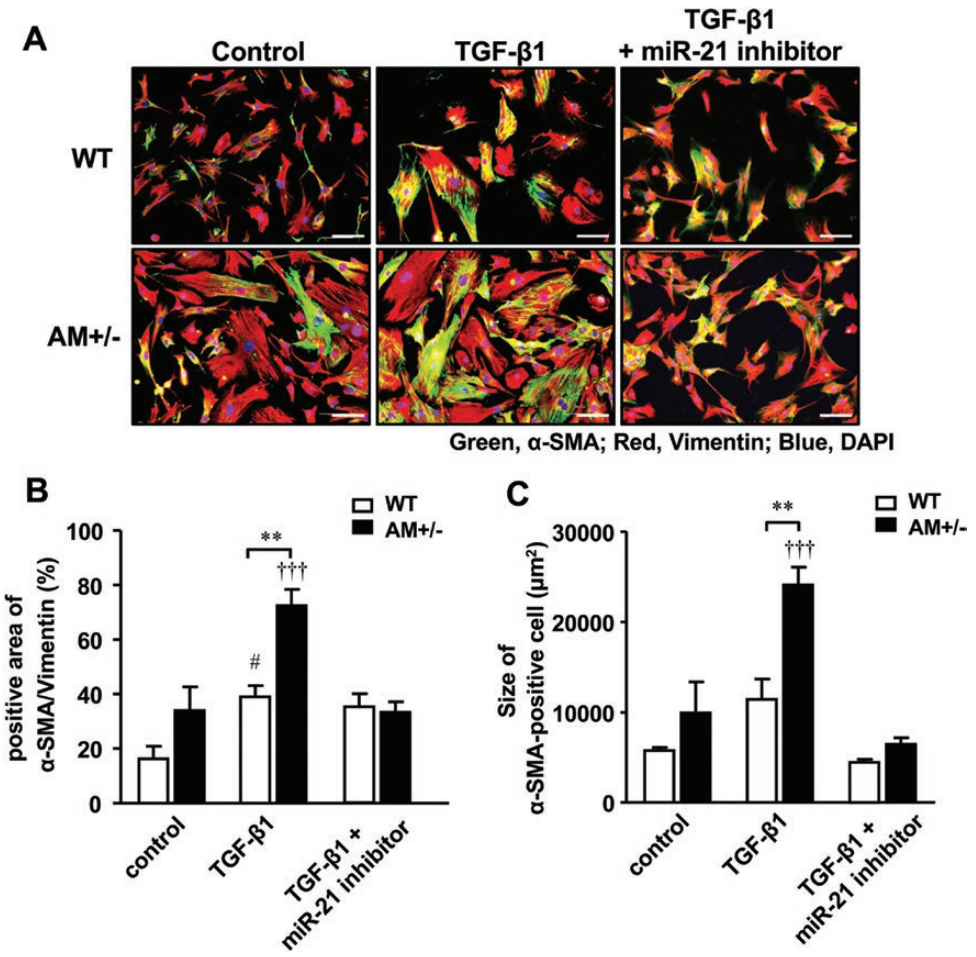

Figure 15. microRNA-21 inhibition suppresses the occurrence of non-p-MyoFbs among TGF-β-stimulated AM+/- fibroblasts. **A,** Representative images of immunostained (Green: α-SMA, Red: vimentin, Blue: DAPI) primary cultured lung fibroblasts isolated from the lungs of AM+/- and WT mice. The cells were grown to 70% confluence. Immunostaining was performed with control and TGF-β1-stimulated (10 ng/mL for 24 hours) cells with or without miR-21 inhibitor. Scale bars = 100 μm. **B,** Percentage α-SMA-positive area / vimentin-positive area. **C,** Size of α-SMA-positive cells. Data are from 3 independent experiments. (**B, C**). Bars are means ± SEM. "*" indicates comparison between the groups, "#" indicates comparison with WT control, "†" indicates comparison with AM+/- control. *P* values were calculated using 2-way ANOVA with Tukey's test.

expression is downregulated, in the lungs of AM+/- mice administered BLM. In our in vitro experiments, we also found that *Mir21* expression is highly upregulated only when AM+/- cells are stimulated with TGF-β and that addition of AM cancels that effect. These observations suggest that AM works to suppress TGF-β-evoked *Mir21* expression and upregulate Smad7 expression. We also confirmed that the effects of inhibiting miR-21 on the differentiation of p-MyoFbs to non-p-MyoFbs were similar to those of AM or TGF-β-Smad3 inhibitors.

Figure 16 summarizes our findings on the effects of the AM-RAMP2 system in the pathogenesis of pulmonary fibrosis. In addition to suppressing inflammation during the early phase, the AM-RAMP2 system also suppresses fibrosis progression by regulating miR-21 expression, the TGF-β-Smads pathway, and non-p-MyoFb differentiation during the chronic phase. These results indicate that the AM-RAMP2 system suppresses the progression of pulmonary fibrosis, making it a promising new target for the treatment of pulmonary fibrosis, for which there are currently limited therapeutic options.

In the treatment of pulmonary fibrosis, pirfenidone and nintedanib are 2 newer drugs that have recently come into use (78). The primary mechanism of action of pirfenidone is inhibition of TGF-β production and suppression of type 2 alveolar epithelial cell differentiation into fibroblasts and myofibroblasts. Nintedanib is a small molecule tyrosine kinase inhibitor that acts on the vascular endothelial growth factor receptor (VEGFR), fibroblast growth factor receptor (FGFR), and platelet-derived growth factor receptor (PDGFR). So far, these drugs have not proved adequately effective and have several adverse side effects. In the context of fibrosis, AM suppresses both inflammation and fibrosis. In addition, because AM is an endogenous bioactive peptide, it is expected to be a safer therapeutic agent than steroids, immunosuppressive agents, anti-inflammatory drugs, or the 2 aforementioned antifibrotic drugs. However, the

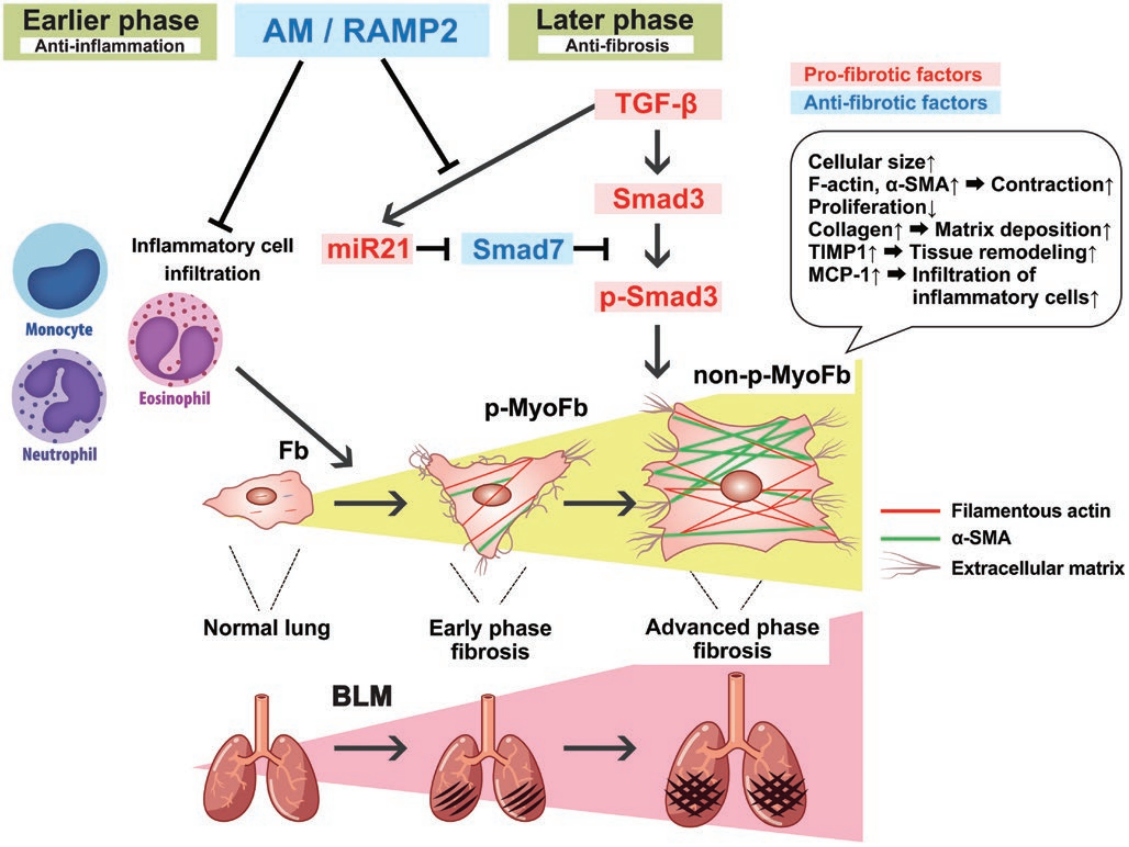

Figure 16. Roles of the AM-RAMP2 system in the pathogenesis of pulmonary fibrosis. During the pathogenesis of pulmonary fibrosis, the AM-RAMP2 system suppresses inflammation during the early acute phase. Later, during the chronic phase, AM-RAMP2 inhibits the progression of fibrosis by suppressing miR-21 expression, signaling in the TGF-β-Smads pathway, and differentiation to nonproliferating myofibroblasts (non-p-MyoFbs).

indications for AM are limited due to its short half-life; AM treatment would require continuous intravenous infusion under hospitalization. In that context, RAMP2 could be an alternative therapeutic target.

Acknowledgments

The authors are grateful to Dr. Shinsuke Taki for valuable comments and to Dr. Kenji Kangawa for providing human recombinant AM.

Financial Support: This study was supported by Grants-in-Aid for Scientific Research (KAKENHI), Core Research for Evolutionary Science and Technology (CREST) of Japan Science and Technology Agency (JST) and the Japan Agency for Medical Research and Development (AMED), a SENSHIN Medical Research Foundation grant, a NOVARTIS Foundation (Japan) for the Promotion of Science grant, an Akaeda Medical Research Foundation grant, a Hoyu Science Foundation grant, a Takahashi Industrial and Economic Research Foundation grant, a Bristol-Myers Squibb research grant, and a The Japan Research Institute of Industrial Science grant to T. Shindo. In addition, funding included a Naito Foundation grant, a Japan Heart Foundation Dr. Hiorshi Irisawa & Dr. Aya Irisawa Memorial Research Grant, a Kanzawa Medical Research Foundation grant, The Uehara Memorial Foundation grant, a Fund of Nagano Prefecture to promote scientific activity, Takeda Science Foundation grant, a Mochida Memorial Foundation for Medical and Pharmaceutical Research grant, and The Nakatomi Foundation grant to M.T.; a NOVARTIS Foundation (Japan) for the Promotion of Science grant to T. Sakurai; and a Yamaguchi Endocrine Research Foundation grant to A.K.; and Y.W. received a scholarship from Japan Student Services Organization.

Author Contributions: Y.W. carried out the experiments and wrote the manuscript. M.T. helped gene expression analysis. T. Sakurai and A.K. generated genetically engineered mice. YI and H.K. helped histological analysis. N.C. and S.K. helped with Western blot analysis. Y.Z. and K.A. helped cwith ellular experiments. H.S. helped with the FACS analysis. T. Shindo planned the experiments and supervised the manuscript.

Additional Information

Correspondence: Takayuki Shindo, MD, PhD, Department of Cardiovascular Research, Shinshu University School of Medicine, Asahi 3-1-1, Matsumoto, Nagano, 390–8621, Japan. Email: tshindo@shinshu-u.ac.jp.

Disclosures: The authors declare no conflicts of interest associated with this manuscript.

Data Availability: Some or all data generated or analyzed during this study are included in this published article or Supplementary data linked this article.

References

1. Yamazaki R, Nishiyama O, Saeki S, Sano H, Iwanaga T, Tohda Y. Characteristics of patients with chronic idiopathic interstitial pneumonia undergoing repeated respiratory-related hospitalizations: a retrospective cohort study. *Plos One*. 2020;**15**(4):e0232212.
2. Disayabutr S, Calfee CS, Collard HR, Wolters PJ. Interstitial lung diseases in the hospitalized patient. *BMC Med*. 2015;**13**:245.
3. Kitamura K, Kangawa K, Kawamoto M, et al. Adrenomedullin: a novel hypotensive peptide isolated from human pheochromocytoma. *Biochem Biophys Res Commun*. 1993;**192**(2):553-560.
4. Ichiki Y, Kitamura K, Kangawa K, Kawamoto M, Matsuo H, Eto T. Distribution and characterization of immunoreactive adrenomedullin in human tissue and plasma. *FEBS Lett*. 1994;**338**(1):6-10.
5. Michibata H, Mukoyama M, Tanaka I, et al. Autocrine/paracrine role of adrenomedullin in cultured endothelial and mesangial cells. *Kidney Int*. 1998;**53**(4):979-985.
6. Kitamura K, Ashizuka S, Inatsu H, Kita T. Adrenomedullin as a potential therapeutic agent for refractory ulcerative colitis. In: Nakao K, Minato N, Uemoto S, eds. *Innovative Medicine: Basic Research and Development*. Springer; 2015:227-240.
7. Ashizuka S, Kuroishi N, Nakashima K, Inatsu H, Kita T, Kitamura K. Adrenomedullin: a novel therapy for intractable Crohn's disease with a loss of response to infliximab. *Intern Med*. 2019;**58**(11):1573-1576.
8. Kita T, Kaji Y, Kitamura K. Safety, tolerability, and pharmacokinetics of adrenomedullin in healthy males: a randomized, double-blind, phase 1 clinical trial. *Drug Des Devel Ther*. 2020;**14**:1-11.
9. Shindo T, Kurihara Y, Nishimatsu H, et al. Vascular abnormalities and elevated blood pressure in mice lacking adrenomedullin gene. *Circulation*. 2001;**104**(16):1964-1971.
10. Niu P, Shindo T, Iwata H, et al. Accelerated cardiac hypertrophy and renal damage induced by angiotensin II in adrenomedullin knockout mice. *Hypertens Res*. 2003;**26**(9):731-736.
11. Niu P, Shindo T, Iwata H, et al. Protective effects of endogenous adrenomedullin on cardiac hypertrophy, fibrosis, and renal damage. *Circulation*. 2004;**109**(14):1789-1794.
12. Tanaka M, Kakihara S, Hirabayashi K, et al. Adrenomedullin-receptor activity-modifying protein 2 system ameliorates subretinal fibrosis by suppressing epithelial-mesenchymal transition in age-related macular degeneration. *Am J Pathol*. 2021;**191**(4):652-668.
13. Nishimatsu H, Hirata Y, Shindo T, et al. Role of endogenous adrenomedullin in the regulation of vascular tone and ischemic renal injury: studies on transgenic/knockout mice of adrenomedullin gene. *Circ Res*. 2002;**90**(6):657-663.
14. Shindo T, Kurihara H, Maemura K, et al. Hypotension and resistance to lipopolysaccharide-induced shock in transgenic mice overexpressing adrenomedullin in their vasculature. *Circulation*. 2000;**101**(19):2309-2316.
15. McLatchie LM, Fraser NJ, Main MJ, et al. RAMPs regulate the transport and ligand specificity of the calcitonin-receptor-like receptor. *Nature*. 1998;**393**(6683):333-339.
16. Shindo T, Tanaka M, Kamiyoshi A, et al. Regulation of cardiovascular development and homeostasis by the adrenomedullin-RAMP system. *Peptides*. 2019;**111**:55-61.
17. Ichikawa-Shindo Y, Sakurai T, Kamiyoshi A, et al. The GPCR modulator protein RAMP2 is essential for angiogenesis and vascular integrity. *J Clin Invest*. 2008;**118**(1):29-39.
18. Koyama T, Ochoa-Callejero L, Sakurai T, et al. Vascular endothelial adrenomedullin-RAMP2 system is essential for vascular integrity and organ homeostasis. *Circulation*. 2013;**127**(7):842-853.
19. Cooper JA Jr. Pulmonary fibrosis: pathways are slowly coming into light. *Am J Respir Cell Mol Biol*. 2000;**22**(5):520-523.
20. Murakami S, Nagaya N, Itoh T, et al. Adrenomedullin regenerates alveoli and vasculature in elastase-induced pulmonary emphysema in mice. *Am J Respir Crit Care Med*. 2005;**172**(5):581-589.
21. Hobara N, Goda M, Kitamura Y, Sendou T, Gomita Y, Kawasaki H. Adrenomedullin facilitates reinnervation of phenol-injured perivascular nerves in the rat mesenteric resistance artery. *Neuroscience*. 2007;**144**(2):721-730.
22. Uetake R, Sakurai T, Kamiyoshi A, et al. Adrenomedullin-RAMP2 system suppresses ER stress-induced tubule cell death and is involved in kidney protection. *Plos One*. 2014;**9**(2):e87667.
23. Imai A, Toriyama Y, Iesato Y, et al. Adrenomedullin suppresses vascular endothelial growth factor-induced vascular hyperpermeability and inflammation in retinopathy. *Am J Pathol*. 2017;**187**(5):999-1015.
24. Hirabayashi K, Tanaka M, Imai A, et al. Development of a novel model of central retinal vascular occlusion and the therapeutic potential of the adrenomedullin-receptor activity-modifying protein 2 system. *Am J Pathol*. 2019;**189**(2):449-466.
25. Eitzman DT, McCoy RD, Zheng X, et al. Bleomycin-induced pulmonary fibrosis in transgenic mice that either lack or overexpress the murine plasminogen activator inhibitor-1 gene. *J Clin Invest*. 1996;**97**(1):232-237.
26. *RRID:AB_2562562*.
27. *RRID:AB_2290801*.
28. *RRID:AB_2629529*.
29. *RRID:AB_2562414*.
30. *RRID:AB_2565852*.
31. *RRID:AB_1236488*.
32. *RRID:AB_2563054*.
33. *RRID:AB_10896143*.
34. *RRID:AB_10563422*.
35. *RRID:AB_1548790*.
36. *RRID:AB_394657*.
37. Shindo T. Data from: adrenomedullin ameliorates pulmonary fibrosis by regulating TGF-β-Smads signaling and myofibroblast differentiation. *Dryad Digital Repository*. Deposited May 21, 2021. doi:10.5061/dryad.5dv41ns5t.
38. *RRID:AB_357485*.
39. *RRID:AB_323806*.
40. *RRID:AB_305055*.
41. *RRID:AB_2223500*.
42. Hubner RH, Gitter W, El Mokhtari NE, et al. Standardized quantification of pulmonary fibrosis in histological samples. *Biotechniques*. 2008;**44**(4):507-511, 514-507.
43. *RRID:AB_10626777*.
44. *RRID:AB_2193182*.
45. *RRID:AB_2193207*.
46. *RRID:AB_2889838*.

47. *RRID:AB_2889839*.
48. *RRID:AB_2223172*.
49. Kono Y, Nishiuma T, Nishimura Y, et al. Sphingosine kinase 1 regulates differentiation of human and mouse lung fibroblasts mediated by TGF-beta1. *Am J Respir Cell Mol Biol*. 2007;**37**(4):395-404.
50. Shimekake Y, Nagata K, Ohta S, et al. Adrenomedullin stimulates two signal transduction pathways, cAMP accumulation and Ca2+ mobilization, in bovine aortic endothelial cells. *J Biol Chem*. 1995;**270**(9):4412-4417.
51. Horio T, Kohno M, Kano H, et al. Adrenomedullin as a novel antimigration factor of vascular smooth muscle cells. *Circ Res*. 1995;**77**(4):660-664.
52. Tanaka M, Koyama T, Sakurai T, et al. The endothelial adrenomedullin-RAMP2 system regulates vascular integrity and suppresses tumour metastasis. *Cardiovasc Res*. 2016;**111**(4):398-409.
53. Kang JH, Jung MY, Choudhury M, Leof EB. Transforming growth factor beta induces fibroblasts to express and release the immunomodulatory protein PD-L1 into extracellular vesicles. *Faseb J*. 2020;**34**(2):2213-2226.
54. Jinnin M, Ihn H, Tamaki K. Characterization of SIS3, a novel specific inhibitor of Smad3, and its effect on transforming growth factor-beta1-induced extracellular matrix expression. *Mol Pharmacol*. 2006;**69**(2):597-607.
55. *RRID:AB_10562134*.
56. *RRID:AB_443209*.
57. Bravo DD, Chernov-Rogan T, Chen J, Wang J. An impedance-based cell contraction assay using human primary smooth muscle cells and fibroblasts. *J Pharmacol Toxicol Methods*. 2018;**89**:47-53.
58. Iesato Y, Toriyama Y, Sakurai T, et al. Adrenomedullin-RAMP2 system is crucially involved in retinal angiogenesis. *Am J Pathol*. 2013;**182**(6):2380-2390.
59. Liu Y, Li Y, Li N, et al. TGF-β1 promotes scar fibroblasts proliferation and transdifferentiation via up-regulating MicroRNA-21. *Sci Rep*. 2016;**6**:32231.
60. Swaisgood CM, French EL, Noga C, Simon RH, Ploplis VA. The development of bleomycin-induced pulmonary fibrosis in mice deficient for components of the fibrinolytic system. *Am J Pathol*. 2000;**157**(1):177-187.
61. Koyama T, Sakurai T, Kamiyoshi A, Ichikawa-Shindo Y, Kawate H, Shindo T. Adrenomedullin-RAMP2 System in Vascular Endothelial Cells. *J Atheroscler Thromb*. 2015;**22**(7):647-653.
62. Giri SN, Hyde DM, Hollinger MA. Effect of antibody to transforming growth factor beta on bleomycin induced accumulation of lung collagen in mice. *Thorax*. 1993;**48**(10):959-966.
63. Wang Q, Wang Y, Hyde DM, et al. Reduction of bleomycin induced lung fibrosis by transforming growth factor beta soluble receptor in hamsters. *Thorax*. 1999;**54**(9):805-812.
64. Nagaraju CK, Robinson EL, Abdesselem M, et al. Myofibroblast Phenotype and Reversibility of Fibrosis in Patients With End-Stage Heart Failure. *J Am Coll Cardiol*. 2019;**73**(18):2267-2282.
65. Hara A, Kobayashi H, Asai N, et al. Roles of the Mesenchymal Stromal/Stem Cell Marker Meflin in Cardiac Tissue Repair and the Development of Diastolic Dysfunction. *Circ Res*. 2019;**125**(4):414-430.
66. Mizutani Y, Kobayashi H, Iida T, et al. Meflin-Positive Cancer-Associated Fibroblasts Inhibit Pancreatic Carcinogenesis. *Cancer Res*. 2019;**79**(20):5367-5381.
67. Li H, Zhao X, Shan H, Liang H. MicroRNAs in idiopathic pulmonary fibrosis: involvement in pathogenesis and potential use in diagnosis and therapeutics. *Acta Pharm Sin B*. 2016;**6**(6):531-539.
68. Dennler S, Huet S, Gauthier JM. A short amino-acid sequence in MH1 domain is responsible for functional differences between Smad2 and Smad3. *Oncogene*. 1999;**18**(8):1643-1648.
69. Gu L, Zhu YJ, Yang X, Guo ZJ, Xu WB, Tian XL. Effect of TGF-beta/Smad signaling pathway on lung myofibroblast differentiation. *Acta Pharmacol Sin*. 2007;**28**(3):382-391.
70. Micallef L, Vedrenne N, Billet F, Coulomb B, Darby IA, Desmoulière A. The myofibroblast, multiple origins for major roles in normal and pathological tissue repair. *Fibrogenesis Tissue Repair*. 2012;**5**(Suppl 1):S5.
71. Desmoulière A, Geinoz A, Gabbiani F, Gabbiani G. Transforming growth factor-beta 1 induces alpha-smooth muscle actin expression in granulation tissue myofibroblasts and in quiescent and growing cultured fibroblasts. *J Cell Biol*. 1993;**122**(1):103-111.
72. Driesen RB, Nagaraju CK, Abi-Char J, et al. Reversible and irreversible differentiation of cardiac fibroblasts. *Cardiovasc Res*. 2014;**101**(3):411-422.
73. Noetel A, Kwiecinski M, Elfimova N, Huang J, Odenthal M. microRNA are Central Players in Anti- and Profibrotic Gene Regulation during Liver Fibrosis. *Front Physiol*. 2012;**3**:49.
74. Loboda A, Sobczak M, Jozkowicz A, Dulak J. TGF-β1/Smads and miR-21 in Renal Fibrosis and Inflammation. *Mediators Inflamm*. 2016;**2016**:8319283.
75. Thum T, Gross C, Fiedler J, et al. MicroRNA-21 contributes to myocardial disease by stimulating MAP kinase signalling in fibroblasts. *Nature*. 2008;**456**(7224):980-984.
76. Liu G, Friggeri A, Yang Y, et al. miR-21 mediates fibrogenic activation of pulmonary fibroblasts and lung fibrosis. *J Exp Med*. 2010;**207**(8):1589-1597.
77. Han M, Wang F, Gu Y, et al. MicroRNA-21 induces breast cancer cell invasion and migration by suppressing smad7 via EGF and TGF-β pathways. *Oncol Rep*. 2016;**35**(1):73-80.
78. Lehmann M, Buhl L, Alsafadi HN, et al. Differential effects of Nintedanib and Pirfenidone on lung alveolar epithelial cell function in ex vivo murine and human lung tissue cultures of pulmonary fibrosis. *Respir Res*. 2018;**19**(1):175.